HHS Public Access

Author manuscript

Mol Cell. Author manuscript; available in PMC 2022 November 04.

Published in final edited form as:

Mol Cell. 2021 November 04; 81(21): 4413–4424.e5. doi:10.1016/j.molcel.2021.08.006.

SPT5 stabilization of promoter-proximal RNA polymerase II

Yuki Aoi[1], **Yoh-hei Takahashi**[1], **Avani P. Shah**[1], **Marta Iwanaszko**[1], **Emily J. Rendleman**[1], **Nabiha H. Khan**[1], **Byoung-Kyu Cho**[1,2], **Young Ah Goo**[1,2], **Sheetal Ganesan**[1], **Neil L. Kelleher**[1,2], **Ali Shilatifard**[1,3,*]

[1]Simpson Querrey Institute for Epigenetics, Department of Biochemistry and Molecular Genetics Feinberg School of Medicine, Northwestern University, Chicago, IL 60611, USA.

[2]Proteomics Center of Excellence, Northwestern University, Evanston, IL 60611, USA.

[3]Lead Contact

Summary

Based on *in vitro* studies, it has been demonstrated that the DSIF complex, comprised of SPT4 and SPT5, regulates the elongation stage of transcription catalyzed by RNA polymerase II (Pol II). The precise cellular function of SPT5 is not clear since conventional gene depletion strategies for SPT5 result in loss of cellular viability. Using an acute inducible protein depletion strategy to circumvent this issue, we report that SPT5 loss triggers the ubiquitination and proteasomal degradation of the core Pol II subunit RPB1, a process which we show to be evolutionarily conserved from yeast to human cells. RPB1 degradation requires the E3 ligase Cullin 3, the unfoldase VCP/p97 and a novel form of CDK9 kinase complex. Our study demonstrates that SPT5 stabilizes Pol II specifically at promoter-proximal regions, permitting Pol II release from promoters into gene bodies providing mechanistic insight into the cellular function of SPT5 in safeguarding accurate gene expression.

Graphical Abstract

*Correspondence to: Ali Shilatifard, Department of Biochemistry and Molecular Genetics, The Louis A. Simpson and Kimberly K. Querrey Biomedical Research Center Room 7-515, 303 East Superior Street, Chicago, IL 60611, USA, Office: (312) 503-5217, ash@northwestern.edu.

Author contributions

Y.A. and A.S. conceived and designed the experiments. Y.A. performed experiments and data analysis in human cells. Y.T. designed and performed experiments in yeast cells. A.P.S and S.G. performed ChIP and cloning. M.I. performed elongation velocity analysis. A.P.S, E.J.R, N.H.K performed sequencing. B.C, Y.G, N.L.K performed proteomics experiments and data processing, and Y.A. analyzed proteomics data. Y.A. and A.S. interpreted results and wrote the manuscript, with input from all authors.

Declaration of interests

The authors declare no competing interests.

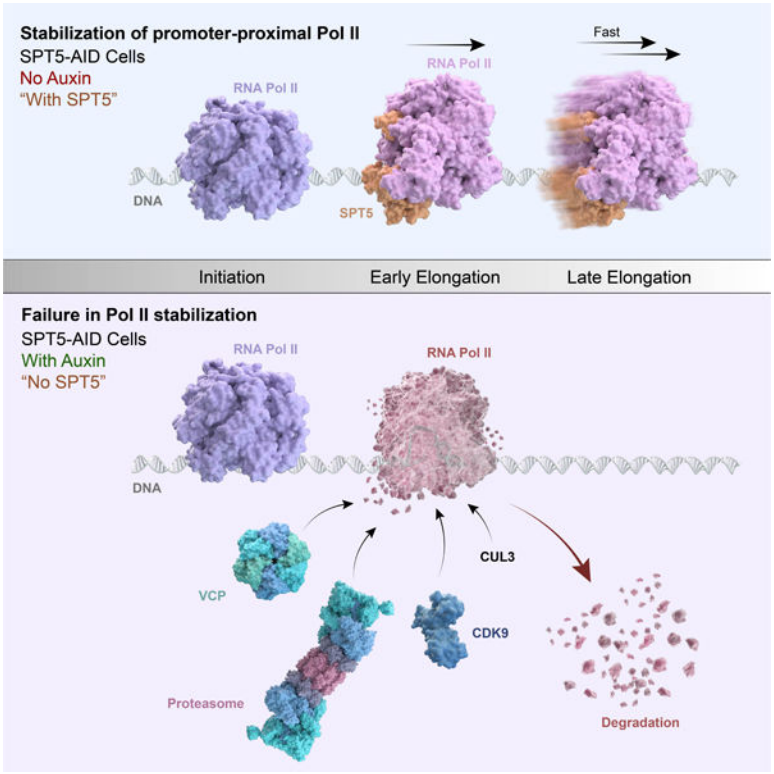

Aoi et al find that the conserved transcription elongation factor SPT5 stabilizes RNA polymerase II (Pol II) in yeast and human cells. SPT5 loss triggers degradation of a Pol II subunit through CUL3, VCP, and CDK9. Stabilizing Pol II may be a SPT5's primary function to safeguard accurate gene expression.

Keywords

Transcription; Elongation; Degradation; RNA polymerase II; SPT5; Cullin 3; CDK9; NELF; VCP; Auxin-inducible degron

Introduction

Transcriptional regulation by RNA polymerase II (Pol II) in eukaryotic cells is a multi-step process regulated by the function of numerous transcription factors safeguarding accurate developmental gene expression (Chen et al., 2018). One such regulated step in gene expression is Pol II elongation control, which includes promoter-proximal pause release and productive elongation (Chen et al., 2018). Promoter-proximal pausing is a specific regulatory step, which immediately follows initiation prior to the productive elongating by Pol II. This step has been shown to be highly regulated and its misregulation is associated with diverse human diseases (Brown et al., 1996; Chen et al., 2018). For Pol II to efficiently transcribe mRNA during the promoter-proximal pause/release and productive elongation stages of transcription, it must overcome physical obstacles such as nucleosomes, be able to be a platform for proper splicing, and deal with many other transcriptional barriers

and impediments (Brown et al., 1996). In so doing, the elongating Pol II associates with numerous factors to safeguard accurate gene expression around such obstacles. However, how cells determine and build a properly equipped Pol II to transverse into the productive elongation stage from the promoter-proximal regions remains largely unknown.

SPT5 is an evolutionarily conserved and essential elongation factor (Decker, 2020). *In vitro* studies demonstrate that SPT5 forms a heterodimer with SPT4, called DSIF, and it is required for pausing and productive elongation (Wada et al., 1998). *In vitro* studies show that a point mutation of SPT5 can lead to failure in pausing, while its elongation activity remains as effective as wild-type (Guo et al., 2000), suggesting that SPT5's roles in pausing and elongation are mechanistically distinct from one other. *In vitro* transcriptional studies also demonstrate that Pol II pausing requires the NELF complex, together with DSIF, by forming the Pol II-DSIF-NELF pausing complex (Yamaguchi et al., 1999; 2002). The structure of this complex has suggested that NELF may restrain Pol II mobility, allowing Pol II to stay in the pausing state (Vos et al., 2018).

Recently, we demonstrated that promoter-proximal Pol II is still paused at the +1 nucleosome-associated regions upon acute depletion of NELF in vivo (Aoi et al., 2020). This suggests that Pol II undergoes a 2-step pausing at promoters: pausing with NELF and pausing at the +1 nucleosome. Supporting this model, depletion of histone variant H2A.Z.1, which is enriched at the +1 nucleosome, has been shown to increase the release of Pol II into gene bodies (Mylonas et al., 2021). In contrast, it has been reported that SPT6 depletion results in the accumulation of Pol II at the +1 nucleosome (Žumer et al., 2021). These acute depletion studies suggest that, in addition to NELF dissociation, there appears to be a regulatory mechanism to promote Pol II release through the +1 nucleosome into gene bodies. These studies also imply that solely looking only at *in vitro* transcriptional studies in test tube may not faithfully recapitulate the in vivo function of such factors and their role in transcriptional control in living cells. Indeed, how SPT5 regulates pausing at the +1 nucleosome remains poorly understood.

Genome-wide studies demonstrate that SPT5 interacts with Pol II throughout the elongation phase (Pavri et al., 2010; Rahl et al., 2010) and it has been proposed that phosphorylation of SPT5 by a positive elongation factor P-TEFb stimulates SPT5's elongation function (Yamada et al., 2006). *In vivo*, P-TEFb predominantly phosphorylates SPT5 at two distinct loci: the C-terminal repeat (CTR) domain and the Kyprides, Ouzounis, Woese (KOW) 4–5 linker region (Sansó et al., 2016). Although CTR phosphorylation promotes productive elongation *in vitro* (Yamada et al., 2006) and *in vivo* (Cortazar et al., 2019; Parua et al., 2018), CTR is dispensable for cell viability (Komori et al., 2009), suggesting that CTR phosphorylation might not be required as a core function of SPT5. Recently, the Integrator Complex coupled with PP2A phosphatase has been shown to remove phosphorylation at the KOW4–5 linker, facilitating premature termination at promoters (Huang et al., 2020).

Although SPT5 has been shown to possess important roles in transcriptional regulation *in vitro*, previous studies to looking at SPT5's *in vivo* function either via RNAi or by gene deletion methods were limited by SPT5 being an essential gene with its depletion resulting in cell death (Fitz et al., 2018; Rahl et al., 2010). Here, we use an acute and rapid depletion

system for SPT5 loss in human cells to dissect the *in vivo* roles in transcription by Pol II. We find a previously unrecognized function for SPT5 and mechanism of action in regulating Pol II stability to facilitate release of Pol II from promoter-proximal regions to gene bodies.

Results

Acute depletion in SPT5 levels leads to RPB1 degradation–

To precisely investigate SPT5 function in living human cells, we generated an auxin-inducible degron (AID) (Natsume et al., 2016) knock-in DLD-1 cell line where the AID-tagged SPT5 is expressed from its endogenous genomic locus. This cell line allowed for the acute depletion of SPT5-AID with ~2 h auxin treatment (Figures 1A and 1B), while avoiding secondary effects of its long-term depletion, including severe growth defect and cell death (Figure S1A). As a control, the untagged SPT5 in parental cells was not degraded by auxin treatment, confirming the AID-dependent degradation in SPT5-AID cells. We noted that following SPT5 depletion, SPT4 levels were somewhat decreased (Figure 1B). This indicates that SPT4 stability depends on SPT5, likely through the formation of the SPT4-SPT5 heterodimer complex DSIF. Unexpectedly, we also observed about an 80% reduction of RPB1, the largest subunit of Pol II, following a decrease in the SPT5 levels (Figure 1B). Other Pol II subunits RPB3 and RPB5 seem to be much more stable upon SPT5 loss (Figures S1B and S1C). While RPB1 and RPB3 are Pol II-specific subunits, RPB5 is a common subunit of Pol I, Pol II and Pol III. This suggests that the stability of RPB5 in the absence of SPT5 may be the result of its incorporation in Pol I and Pol III.

To determine if RPB1 loss is a general phenomenon or specific to SPT5, we next treated NELF-C-AID, NELF-E-AID (Aoi et al., 2020), PAF1-AID (Chen et al., 2017), and SPT4-AID cells with auxin and tested for Pol II stability within the same time frame as SPT5. Interestingly, neither PAF1, NELF, nor SPT4 depletion affected RPB1 levels similar to SPT5 depletion (Figures 1C, 1D, S1D, S1E), strongly suggesting that regulation of RPB1stability is a SPT5-specific function and not a general function of elongation factors. We noted that SPT5 levels are slightly decreased upon SPT4-AID degradation, but a significant amount of SPT5 remained compared with depletion levels of SPT5-AID (Figure S1E). It is likely that the remaining amount of SPT5 is sufficient to maintain RPB1 stability in the absence of SPT4. We also demonstrated that inhibition of protein synthesis still resulted in the observed RPB1 loss (Figure 1E), revealing that SPT5 depletion results in RPB1 degradation.

To further examine the degradation dynamics of RPB1, we prepared nucleoplasmic and chromatin fractions from auxin-treated SPT5-AID cells. As observed in whole-cell extracts, total RPB1 levels were decreased in both nucleoplasmic and chromatin fractions (Figure S2A). To test if SPT5 depletion affects phosphorylation status of RPB1, we blotted for phosphoserine 2 (S2P) and phosphoserine 5 (S5P) of the C-terminal domain (CTD) of RPB1. Interestingly, S5P levels were less stable than S2P levels as total RPB1 levels were decreased (Figure S2A). This suggests that RPB1-S5P may be preferentially targeted for degradation upon SPT5 depletion.

Cul3 ubiquitin ligase, VCP unfoldase and the proteasome are associated with Pol II upon SPT5 depletion–

SPT5 physically interacts with Pol II (Wada et al., 1998) and co-localizes with Pol II at most transcriptionally active genes on chromatin (Pavri et al., 2010; Rahl et al., 2010), suggesting that chromatin-bound Pol II complexes mostly exist with SPT5. We reasoned that SPT5 depletion may affect the protein-protein interaction properties/composition of Pol II transcription units, which can trigger the RPB1 degradation pathway. To examine relative amounts of Pol II interacting proteins, we immunoprecipitated the endogenous Pol II complex from nuclease-digested chromatin fraction and identified co-immunoprecipitated proteins by mass spectrometry, both in the presence and absence of SPT5 (Figures S2B-D, Table S1). We normalized protein levels to Pol II abundance in each condition, since RPB1 is partially degraded in chromatin fraction after auxin treatment for 2 h (Figure S2A, S2D). As expected, SPT5 and SPT4 levels were significantly decreased upon auxin treatment in these purifications (Figure 2A), which validates our mass spectrometric quantification method. We observed a reduction of elongation factor ELOF1 (Figure 2A), which is consistent with its known interaction with SPT5 and Pol II (Ehara et al., 2019). Cap methyltransferase CMTR1 was also reduced, suggesting a possible role for SPT5 in CMTR1 recruitment similar to the recruitment of capping enzyme by SPT5 (Doamekpor et al., 2014). We observed that levels of other Pol II associating complexes were largely unchanged (Figure 2B).

Strikingly, we observed a significant enrichment of 3 factors involved in degradation pathways among increased proteins: a ubiquitin ligase Cullin 3 (CUL3), an unfoldase VCP/p97, and a proteasome subunit PSMD12/RPN5 (Figure 2A, Table S1). Since the proteasome can be recruited by the SPT5-AID degradation process, we focused on CUL3 and VCP's possible roles in RPB1 degradation below.

CUL3 is required for RPB1 degradation as the result of SPT5 depletion–

CUL3 is one of the human Cullin family proteins that serve as scaffolds of Cullin-RING E3 ubiquitin ligase complexes (Chen and Chen, 2016). To date, a CUL3's role in RPB1 degradation has not been reported in metazoans. To examine a CUL3's role in RPB1 degradation, we performed shRNA against CUL3. We found that CUL3 knockdown using 2 independent shRNA constructs partially stabilized RPB1 upon SPT5 depletion (Figure 3A, S3A). Importantly, CUL3 knockdown did not affect SPT5-AID degradation. Indeed, AID degradation requires an E3 ligase CUL1 (Natsume et al., 2016), but not CUL3. Hence, our knockdown experiments demonstrate CUL3-dependent degradation of RPB1, which is mechanistically distinct from CUL1-dependent degradation of SPT5-AID. This finding rules out the possibility of co-degradation of RPB1 and SPT5-AID by CUL1 upon auxin treatment. Also, we do not think that co-degradation of RPB1 is a possibility as AID of other elongation factors such as NEFL, PAF1, SPT6 and other elongation factors does result in RPB1 degradation (Figures 1 and S1).

We next performed chromatin immunoprecipitation sequencing (ChIP-seq) with spike-in normalization for Pol II to explore the Pol II stability on chromatin. Upon SPT5 loss, we observed a strong accumulation of Pol II signal at 5' ends of genes when depleting CUL3

(Figures 3B and 3C), indicating that CUL3 is required for RPB1 degradation on chromatin in the absence of SPT5.

It has been shown that DNA damage induces RPB1 degradation, which requires E3 ubiquitin ligase NEDD4 (Anindya et al., 2007), or CUL5 (Yasukawa et al., 2008). Unexpectedly, knockdown of NEDD4 or CUL5 did not stabilize RPB1 upon SPT5 loss (Figures 3A–3C, S3B). Overall, our results indicate that CUL3, but not NEDD4 or CUL5, is required for RPB1 degradation in the absence of SPT5.

To further examine CUL3's role in RPB1 degradation, we performed ChIP-seq for CUL3. In the untreated condition, CUL3 signal was barely detectable on chromatin via ChIP (Figure 3D, S3C). Interestingly, Auxin treatment for 1.5 h led to increased CUL3 signal at gene regions, and notably, the increased CUL3 signal overlaps Pol II ChIP-seq signal genome-wide (Figure 3D). RPB1 was partially degraded at this treatment time (Figure S3A). This ChIP-seq result is consistent with our proteomics data, where the amount of Pol II-associated CUL3 was increased upon SPT5-AID degradation. We validated the CUL3 ChIP-seq signal by CUL3 knockdown experiments (Figure S3C, D). Together, our data strongly suggests CUL3-Pol II association on chromatin that is triggered by SPT5-AID degradation.

VCP activity is required for RPB1 degradation as the result of SPT5 depletion–

VCP is known to mediate the unfolding of ubiquitylated proteins through its ATPase activity, leading to efficient protein degradation (van den Boom and Meyer, 2018). To test if VCP is required for RPB1 degradation upon SPT5 loss, we performed shRNA against VCP. VCP depletion by 2 independent shRNA constructs appeared to partially stabilize RPB1 in the absence of SPT5 (Figure 4A). To further confirm this result, we treated SPT5-AID cells with NMS-873 (Magnaghi et al., 2013), a potent inhibitor of the VCP ATPase activity. The pharmacological inhibition of VCP significantly stabilized RPB1 upon SPT5 loss (Figure 4B and S4A), indicating that the VCP ATPase activity is required for RPB1 degradation in the absence of SPT5.

It has been shown that a defect in Pol II initiation causes RPB1 degradation (Titov et al., 2011; Vispé et al., 2009). Whereas SPT5 is known to regulate elongation (Wada et al., 1998), a recent report has suggested that SPT5 also regulates initiation (Diamant et al., 2016). This prompted us to test whether an initiation defect induces VCP-mediated RPB1 degradation. Unexpectedly, the VCP inhibition did not stabilize RPB1 when inhibiting initiation by triptolide (TPL) (Figure 4C). This result revealed that there are at least two distinct RPB1 degradation pathways: (1) VCP-dependent degradation induced by SPT5 depletion, and (2) VCP-independent degradation induced by TPL-stimulated initiation defect. By dissecting these two degradation pathways, we concluded that in the absence of SPT5, RPB1 is degraded either during the early (promoter-proximal regions) or during the productive elongation stage, but not during the initiation stage.

Evolutionary conservation of RPB1 degradation pathway in the absence of SPT5 from yeast to human–

SPT5 and VCP are evolutionarily conserved proteins among eukaryotes (van den Boom and Meyer, 2018; Wada et al., 1998). To examine if the SPT5-VCP pathway for RPB1 degradation is conserved in other organisms, we generated *Saccharomyces cerevisiae* strains where SPT5, or a combination of Cdc48 (a yeast ortholog of VCP) and SPT5 can be rapidly depleted from nuclei using the anchor-away technique (Haruki et al., 2008). Surprisingly, SPT5 depletion led to RPB1 loss, and Cdc48 co-depletion suppressed this RPB1 loss (Figure S4B). Collectively, our experiments suggest an evolutionarily conserved function of SPT5 in stabilizing Pol II.

Promoter-proximal Pol II's stability is regulated by SPT5–

To determine how SPT5 depletion and VCP inhibition affect the steady-state of transcription by Pol II, we treated SPT5-AID cells with the VCP inhibitor, followed by auxin, then performed ChIP-seq for Pol II. In the absence of SPT5, peaks of Pol II were barely detected as compared to the vehicle control (Figures 5A, 5B, S5A), likely due to RPB1 degradation. We asked whether the loss of Pol II signal as the result of SPT5 depletion could be suppressed by VCP inhibition. As shown (Figures 5A, 5B, S5A), VCP inhibition restored Pol II levels on chromatin in the absence of SPT5. ChIP-seq for SPT5 showed that SPT5 signal was barely detectable upon SPT5 depletion even when inhibiting VCP (Figures 5A, 5B), which confirmed nearly complete depletion of SPT5 from chromatin. These SPT5 depletion experiments coupled with VCP inhibition allowed us to directly investigate how SPT5 regulates Pol II transcription on chromatin, while avoiding Pol II loss due to RPB1 degradation. Careful analysis of the ChIP-seq data suggested that Pol II levels were strongly accumulated at the 5' end of gene bodies in the absence of SPT5 and in the presence of VCP inhibitors (Figures 5A, 5B, S5A). In contrast, Pol II at the rest of gene bodies appear to show normal distribution pattern (Figures 5A, S5A). This indicates that RPB1 degradation induced by SPT5 loss occurs during the early stage of elongation. Interestingly, we also observed RPB1 loss during early elongation in yeast, and co-depletion of Cdc48 rescued this RPB1 loss (Figures S5B, S5C), suggesting an evolutionary conserved mechanism of Pol II stabilization by SPT5 during early elongation.

SPT5 loss specifically results in the loss of stability of promoter-proximal Pol II and not Pol II in the productive elongation stage–

To gain further insight into how SPT5 depletion and VCP inhibition affect dynamics of Pol II transcription during different stages of elongation, we performed a pulse-chase nascent RNA labeling assay to determine the faith of both early (promoter-proximal) and late (productive elongation) elongating Pol II. In this assay, we treated SPT5-AID cells with P-TEFb inhibitor NVP-2 for 1 h, followed by *in vivo* nascent RNA labeling with 4-thiouridine (4sU). The P-TEFb inhibition blocks pause/escape, but does not alter the elongation form of Pol II that has already escaped (Jonkers et al., 2014), allowing us to infer a distance that Pol II travels during P-TEFb inhibition in the presence or absence of SPT5. By transient transcriptome sequencing (TT-seq) (Schwalb et al., 2016), we mapped genome-wide localization of 4sU-labeled nascent RNA. Surprisingly, Pol II was able to

travel substantial distances when SPT5 was depleted, although this distance is shorter than that of the untreated control (Figures 5C, 5D). This suggests that Pol II at the late elongation stage is unlikely to be degraded in the absence of SPT5. We then estimated the elongation velocity in a time-course treatment of NVP-2 (0, 30, 60 min) (Figure S5D) at the single gene level (Figure 5E) and meta-gene level (Figure S5E). While the Pol II velocity in the untreated condition is consistent with previously reported velocities for Pol II (Jonkers et al., 2014), the velocity of SPT5-depleted Pol II was significantly slower (Figures 5E, S5E). Interestingly, stabilization of Pol II by VCP inhibition did not rescue this slower velocity (Figures 5E, S5E). This indicates that even when Pol II is stabilized at promoter proximal regions, SPT5 is required for proper elongation velocity during the late elongation stage on the body of the genes. Collectively, our steady-state and pulse-chase analyses for Pol II, together with dissection of degradation pathways, demonstrated that VCP-dependent RPB1 degradation upon SPT5 loss does not occur during the initiation stage or the fully productive elongation stage but rather during the early promoter-proximal stage. This conclusion is consistent with our finding that S5P, which is associated with promoter-proximal Pol II, may be a target of degradation (Figure S2A).

Acute depletion of SPT5 leads to pausing transition–

We recently demonstrated that NELF functions *in vivo* by regulating the transition of pausing states rather than escape from promoter-proximal pausing (Aoi et al., 2020). Upon NELF loss, Pol II elongation travels from the first pause region before pausing at a second pause region corresponding to the +1 nucleosomal dyad (Aoi et al., 2020). We reasoned that the SPT5 depletion system coupled with the VCP inhibition described above may allow us to precisely investigate SPT5 function in promoter-proximal pause/release. We performed precision run-on sequencing (PRO-seq) with spike-in normalization (Kwak et al., 2013) to map the Pol II positions at base-pair resolution. Strikingly, Pol II was paused at the second pause regions when depleting SPT5 and inhibiting VCP (Figures 5F–5H), which resembles NELF depletion. We then performed ChIP-seq for the NELF-A subunit and observed a strong reduction of NELF-A signal when depleting SPT5 and inhibiting VCP (Figure 5I). We noted that in this condition, the residual NELF-A signal at promoters was detected (Figure 5I), suggesting a weak NELF-Pol II interaction in the absence of SPT5. Collectively, these results indicate that SPT5 regulates promoter-proximal pausing at the first pause region likely through its interaction with NELF, and that the transition to the second pause region upon SPT5 depletion is through NELF dissociating from Pol II.

A distinct Cdk9 complex is required for RPB1 degradation induced by SPT5 depletion–

To further understand the mechanism of RPB1 degradation during early elongation, we interrogated the requirement for Cdk9/P-TEFb, which positively regulates the release from promoter-proximal pausing at most Pol II-transcribed genes (Chen et al., 2018). We treated SPT5-AID cells with the CDK9 inhibitor NVP-2, followed by auxin, then performed ChIP-seq for Pol II. Surprisingly to us, CDK9 inhibition stabilized a substantial amount of Pol II in the absence of SPT5 (Figure 6A). Pol II signals were mostly accumulated at the 5’ ends of gene bodies (the promoter-proximal regions) (Figures 6A–6C). To further confirm this result, we used THAL-SNS-032, a degrader of CDK9 (Olson et al., 2018). The pharmacological degradation of CDK9 also stabilized Pol II levels (Figures 6A–6C, S6A).

Thus, these results suggest that CDK9/P-TEFb function is required for RPB1 degradation at the promoter-proximal regions in the absence of SPT5. Interestingly, RPB1 was not stable when SPT5 was first depleted followed by CDK9 inhibition (Figure S6B). This suggests that CDK9 is required for RPB1 degradation when SPT5 depletion triggers it.

P-TEFb forms multiple distinct catalytically active complexes with specific functions within each complex (Zheng et al., 2021). For example, SEC-P-TEFb is required for rapid transcriptional induction as the result of heat shock (Lin et al., 2010; Zheng et al., 2021), while BRD4-P-TEFb is required for general transcription (Jang et al., 2005; Yang et al., 2005; Zheng et al., 2021). We, therefore, examined the dependence of P-TEFb on SEC or BRD4 in Pol II degradation when depleting SPT5. Unexpectedly, the pharmacological inhibition of SEC-P-TEFb interaction (Liang et al., 2018) or degradation of BRD4 (Winter et al., 2017) did not stabilize RPB1 upon SPT5 loss (Figure 6D), unlike the use of general P-TEFb inhibitors as shown (Figures 6A and 6B). This unexpected finding suggests that a novel form of P-TEFb complex activated by an unknown factor other than SEC or BRD4 regulates RPB1 degradation in the absence of SPT5.

Discussion

This study provides detailed mechanistic and biochemical insight into in vivo functions of SPT5. Stabilization of promoter-proximal Pol II by SPT5 is a crucial step to release Pol II into gene bodies (Figure 7A). This regulatory step connects proper transition from transcriptional initiation to productive elongation to safeguard accurate gene expression. SPT5 is also required for promoter-proximal pausing through NELF recruitment, and proper elongation velocity. It is important to argue that what comes first in the absence of SPT5: destabilization of Pol II, pausing defect, or slower velocity. An intriguing possibility is that SPT5 loss leads to unproductive elongation on nucleosomes, which may trigger RPB1 destabilization. Indeed, upon DNA damage, Pol II stalls at transcription-blocking lesions and this triggers RPB1 destabilization (Gregersen and Svejstrup, 2018). There may be a common mechanism to recognize elongation-incompetent Pol II on chromatin, although distinct E3 ligases are used for RPB1 degradation in each case. Interestingly, NELF depletion does not lead to RPB1 degradation (Figure 1C) while Pol II being incapable of traversing the +1 nucleosome (Aoi et al., 2020), and PAF1 depletion does not lead to RPB1 degradation (Figure 1D) while reducing elongation velocity in long genes (Chen et al., 2017; Hou et al., 2019). These findings suggest that pausing defect or slower velocity may not necessarily lead to RPB1 degradation. This raises another possibility that SPT5 may regulate RPB1 stability and proper elongation (pausing and velocity) independently. Future studies will dissect these possibilities and elucidate the order of events that is triggered by SPT5 depletion.

It is interesting that SPT5 depletion leads to destabilization of promoter-proximal Pol II but NELF depletion does not, while both depletions result in pausing shift to the + 1 nucleosome (Aoi et al., 2020). One of the major differences is that SPT5 depletion leads to NELF loss, but NELF depletion does not lead to SPT5 loss (Aoi et al., 2020). This raises the possibility that SPT5 protects promoter-proximal Pol II from RPB1 degradation in the absence of NELF (Figure 7B). This model is consistent with the previous finding that NELF-depleted

Pol II undergoes premature termination at promoter-proximal regions (Aoi et al., 2020), rather than destabilization of Pol II. It is likely that Pol II is capable of termination as long as SPT5 interacts with it.

We identify the ubiquitin ligase CUL3 as a novel proteolysis machinery targeting RPB1 in the absence of SPT5 (Figures 2, 3, 7A). We also show that neither NEDD4 nor CUL5 is required for this RPB1 degradation (Figure 3), while NEDD4 or CUL5 is required for damage-induced RPB1 degradation (Anindya et al., 2007; Yasukawa et al., 2008). These results reveal that the CUL3-RPB1 degradation pathway in the absence of SPT5 is distinct from the damage-induced RPB1 degradation pathway. Intriguingly, the VCP unfoldase is required for both degradation pathways (Figure 4) (Gregersen and Svejstrup, 2018; He et al., 2017). We speculate that cells may use different ligases for RPB1 ubiquitylation in a context-dependent manner, while removal of ubiquitylated RPB1 from chromatin generally depends on the unfolding function of VCP.

How the degradation machinery recognizes RPB1 upon SPT5 loss remains unknown. When depleting SPT5 and inhibiting VCP, while Pol II was accumulated at the 5’ end of genes, Pol II distribution at the rest of gene bodies was surprisingly normal (Figure 5). Our data also demonstrate that Pol II can persist in late elongation stage in the absence of SPT5 (Figure 5). These features may distinguish the SPT5-RPB1 degradation pathway from previously reported RPB1 degradation pathways, where Pol II is irreversibly stalled by DNA lesions, Pol II inhibitors, or the inability to resolve backtracked Pol II (Gregersen and Svejstrup, 2018). Intriguingly, a recent study has predicted that SPT5 may block the recruitment of yeast Rad26 to lesion-stalled Pol II upon DNA damage (Xu et al., 2017). SPT5 loss may improperly stimulate recruitment of a degradation apparatus including Rad26 to Pol II. One could speculate that SPT5 acts as a physiological switch of RPB1 degradation.

We show that an initiation defect stimulates an alternative RPB1 degradation pathway in a VCP-independent manner (Figure 4). Although it is unknown how RPB1 is degraded without VCP’s function, our data underline multiple degradation pathways for RPB1. We assume that upon inhibition of initiation, RPB1 predominantly exists as a free form in the nucleoplasm, since chromatin-bound Pol II undergoes termination. This free RPB1 may be rapidly degraded without the unfolding function of VCP. Intriguingly, the maintenance of the free Pol II levels is associated with human diseases such as Cockayne syndrome (Tufegdžić Vidaković et al., 2020), highlighting a physiological significance of the VCP-independent Pol II stability.

Our data suggest that a CDK9 complex, perhaps with an unknown activator other than SEC or BRD4, is required for RPB1 degradation upon SPT5 (Figure 6). Although CDK9 is known to be activated by SEC and BRD4 and inactivated by HEXIM-7SK small nuclear ribonucleoprotein particle complex (Chen et al., 2018), how CDK9 regulates Pol II transcription without SEC or BRD4 remains unknown. Future *in vivo* studies will identify an active form of CDK9 complex as well as its target phosphorylation sites that are required for RPB1 degradation in the absence of SPT5.

We demonstrate that the SPT5-VCP pathway for RPB1 stability is functionally conserved in yeast *Saccharomyces cerevisiae* and human cells (Figures 4 and S4). In yeast *Schizosaccharomyces pombe*, an acute depletion of SPT5 has been shown to change the distribution of Pol II, resulting in an accumulation at 5' end of genes and decreased Pol II levels downstream (Shetty et al., 2017). Interestingly, total RPB1 levels appear to remain relatively unchanged after SPT5 depletion in *S. pombe* (Shetty et al., 2017). Since *S. pombe* and *S. cerevisiae* show distinct regulations for Pol II transcription (Booth et al., 2016), it is possible that depletion of *S. pombe* SPT5 only affects Pol II distribution, but does not trigger RPB1 degradation. However, we cannot rule out the contribution of experimental differences in the two studies. Future studies using different organisms with acute depletion methods will be needed to explore the conservation of RPB1 degradation in the absence of SPT5.

Intriguingly, establishment of promoter-proximal pausing is a metazoan-specific function of SPT5. In *S. cerevisiae*, Pol II appears not to undergo a promoter-proximal pausing step (Steinmetz et al., 2006), and its genome lacks the pausing factor NELF (Narita et al., 2003). Together with these findings, our work suggests that the stabilization of Pol II is one of SPT5's primary functions in eukaryotes, while metazoans have acquired promoter-proximal pausing as a secondary regulatory function.

Limitations of the Study

We show evidence for CUL3-RPB1 interaction by proteomics and ChIP-seq experiments, but our data cannot exclude the possibility that this interaction is indirect. To test if the CUL3-RPB1 interaction is direct, it is crucial to identify a substrate recognition subunit of the CUL3-RING complex among nearly 200 candidate subunits in the human genome(Dubiel et al., 2018). It is also possible that CUL3 recognizes another Pol II subunit or Pol II associated proteins to target RPB1 degradation in the absence of SPT-5. The AID system allows for gene-specific depletion, unlike shRNA knockdown having off-target effects. We show that in parental cells (no AID tag), auxin treatment does not lead to RPB1 degradation. This control is sufficient to claim that SPT5-AID depletion leads to RPB1 degradation. It would be interesting to test if a disruption of SPT5-RPB1 interaction leads to RPB1 degradation by rescue experiments.

STAR Methods text

RESOURCE AVAILABILITY

Lead contact—Further information and requests for reagents may be directed to and will be fulfilled by the Lead Contact, Ali Shilatifard (ASH@Northwestern.edu).

Materials availability—Unique reagents generated in this study are available from the Lead Contact without restriction.

Data and code availability

- Sequencing data and proteomics data have been deposited at GEO and ProteomeXchange respectively and are publicly available as of the date of publication. Accession numbers are listed in the key resources table.

- This paper does not report original code.
- Any additional information required to reanalyze the data reported in this paper is available from the lead contact upon request.

EXPERIMENTAL MODEL AND SUBJECT DETAILS

Human cell lines—Human DLD-1 cells were cultured at 37°C in DMEM (Sigma #D6429) supplemented with 10% FBS (Sigma #F2442), 1% Pen-Strep (Gibco #15140–122) in CO2 incubators. SPT5-AID DLD-1 and SPT4-AID DLD-1 cells were prepared with miniAID/IAA17 tag (Natsume et al., 2016) as described previously (Aoi et al., 2020): Briefly, DLD-1 parental cells that constitutively express OsTIR1 (Holland et al., 2012) were co-transfected with 2 donor plasmids (NeoR and HygR markers) and 1 gRNA-Cas9 plasmid. Clones showing resistance to 250 μg/ml Geneticin (Gibco #10131–027) and 100 μg/ml Hygromycin B (Invitrogen #10687010) were isolated. Homozygous tagging at C-terminus of the targeted gene was validated by PCR and western blotting. SPT5-AID^{7} DLD-1 cells were prepared with miniIAA7 tag and AtAFB2 as described previously (Li et al., 2019) with some modifications. To knock-in miniIAA7 tag and the AtAFB2 gene at the same time, DLD-1 cells (ATCC #CCL-221) were co-transfected with 2 donor plasmids that contain miniIAA7 tag with AtAFB2-P2A-NeoR or AtAFB2-P2A-HygR, and 1 gRNA-Cas9 plasmid. Clones were selected and validated as described above. To induce degradation of AID or AID^{7}-tagged proteins, 500 μM auxin was added to culture.

For shRNA experiments, 293T cells were co-transfected with a pGIPZ shRNA plasmid (Horizon Discovery) with psPAX2 and pMD2.G to package lentivirus, followed by concentration of lentivirus using 4x Lentivirus concentrator (40% PEG-8000, 1.2 M NaCl in PBS). Cells were infected with shRNA virus in the presence of 8 μg/ml polybrene (Sigma #TR-1003-G). After 4–6 days post-infection, cells were used for time-course auxin treatment.

Yeast cell lines—Yeast cells used in this study are derived from HHY168 (Haruki et al., 2008). Spt5-FRB cells are constructed with standard yeast transformation technique through homologous recombination-mediated insertion of PCR-amplified FRB-KanMX6 fragments into the C-terminus of Spt5. Spt5-FRB Cdc48-FRB double anchor-away cells are constructed similarly with FRB-GFP-His3MX6 fragments insertion into the C-terminus of Cdc48 from Spt5-FRB cells. pFA6a-FRB-KanMX6 and pFA6a-FRB-GFP-His3MX6 plasmids for PCR amplification were obtained from Euroscarf.

METHOD DETAILS

Pol II immunoprecipitation—~20 million cells were lysed in lysis buffer (10 mM Tris-HCl pH 7.4, 10 mM KCl, 1.5 mM MgCl2, 12% Sucrose, 10% Glycerol, 0.2% Triton X-100, 0.5 mM DTT, Protease inhibitors (ThermoFisher # A32965), Phosphatase inhibitors (ThermoFisher # A32957)), then fractionated in sucrose cushion (10 mM Tris-HCl pH 7.4, 10 mM KCl, 1.5 mM MgCl2, 30% Sucrose, 0.5 mM DTT). Nuclei were stored in freeze buffer (10 mM Tris-HCl pH 7.4, 10 mM KCl, 1.5 mM MgCl2, 40% Glycerol, 0.5 mM DTT) at –80°C.

Chromatin DNA/RNA was digested in Chromatin digestion buffer (20 mM Tris-HCl pH 7.4, 150 mM NaCl, 1.5 mM MgCl2, 10% Glycerol, 0.05% IGEPAL, 0.5 mM DTT, Protease inhibitors (ThermoFisher # A32965), Phosphatase inhibitors (ThermoFisher # A32957), 250 U/ml Benzonase (Sigma #E1014)). After centrifugation, the supernatant was collected as fraction 1, while proteins were further extracted from the pellet in Chromatin-2 buffer (20 mM Tris-HCl pH 7.4, 500 mM NaCl, 1.5 mM MgCl2, 10% Glycerol, 0.05% IGEPAL, 0.5 mM DTT, Protease inhibitors, Phosphatase inhibitors, 3 mM EDTA) as fraction 2. NaCl concentration in fraction 2 was adjusted to ~150 mM, then combined with fraction 1. Pol II immunoprecipitation was performed using a monoclonal antibody against Pol II CTD (clone 4H8, Cell signaling # 2629S), conjugated to Protein G Dynabeads (Invitrogen # 10004D). After washing with wash buffer (20 mM Tris-HCl pH 7.4, 225 mM NaCl, 1.5 mM MgCl2, 10% Glycerol, 1.5 mM EDTA, 0.05% IGEPAL, 0.5 mM DTT), immunoprecipitated proteins were eluted in mild elution buffer (0.1% SDS, 50 mM Tris-HCl pH 8.0, 1 mM EDTA).

Proteomics Sample Preparation—Samples were run on SDS-PAGE gel and a gel band was subject for in-gel digestion. Gel band was washed in 100 mM Ammonium Bicarbonate (AmBic)/Acetonitrile (ACN) and reduced with 10 mM dithiothreitol at 50°C for 30 minutes. Cysteines were alkylated with100 mM iodoacetamide in the dark for 30 minutes in room temperature. Gel band was washed in 100mM AmBic/ACN prior to adding 600 ng trypsin for overnight incubation at 37 °C. Supernatant contain peptides was saved into a new tube. Gel was washed at room temperature for ten minutes with gentle shaking in 50% ACN/5% FA, and supernatant was saved to peptide solution. Wash step was repeated each by 80% ACN/5% FA, and 100% ACN, and all supernatant was saved then subject to the speedvac dry. After lyophilization, peptides were reconstituted with 5% ACN/0.1% FA in water.

LC-MS/MS Analysis—Peptides were analyzed by LC-MS/MS using a Dionex UltiMate 3000 Rapid Separation nanoLC coupled to a Orbitrap Elite Mass Spectrometer (Thermo Fisher Scientific Inc, San Jose, CA). Samples were loaded onto the trap column, which was 150 μm x 3 cm in-house packed with 3 um ReproSil-Pur® beads. The analytical column was a 75 um x 10.5 cm PicoChip column packed with 3 um ReproSil-Pur® beads (New Objective, Inc. Woburn, MA). The flow rate was kept at 300nL/min. Solvent A was 0.1% FA in water and Solvent B was 0.1% FA in ACN. The peptide was separated on a 120-min analytical gradient from 5% ACN/0.1% FA to 40% ACN/0.1% FA. MS^1 scans were acquired from 400–2000m/z at 60,000 resolving power and automatic gain control (AGC) set to 1×10^6. The 15 most abundant precursor ions in each MS^1 scan were selected for fragmentation by collision-induced dissociation (CID) at 35% normalized collision energy in the ion trap. Previously selected ions were dynamically excluded from re-selection for 60 seconds. Samples were analyzed in biological triplicates.

ChIP-seq—Library preparation and data analysis for ChIP-seq in human DLD-1 cells with mouse spike-in normalization were performed as described previously (Aoi et al., 2020) with minor modification. Briefly, 20–50 million DLD-1 cells were crosslinked with 1% paraformaldehyde (Electron Microscopy Sciences) in PBS for 10 min at r.t. Following addition of spike-in mouse embryonic fibroblast fixed cells, chromatin was sonicated with the Covaris E220. DNA-protein crosslinked complexes were immunoprecipitated overnight

at 4C with antibodies (RPB1 NTD antibody for human Pol II, please see antibodies section) and Dynabeads Protein G (Invitrogen). Protease treatment and reverse crosslinking reaction were performed at 65 °C overnight, followed by DNA purification using PCR purification kit (QIAGEN). DNA libraries were sequenced on the NovaSeq 6000 (Illumina). Low-quality bases were removed from 3' ends using cutadapt 1.14 (Martin, 2011). Reads were aligned to a concatenated genome consisting of human hg38 and mouse mm10 assembly using bowtie 2.2.6 (Langmead and Salzberg, 2012) with –sensitive option. The aligned reads with MAPQ ≥ 30 were extended to 150 bp and read counts were normalized to total reads aligned to spike-in genome.

In *S. cerevisiae*, yeast cells were grown in YPAD medium. Exponentially growing yeast cultures were treated with 1.0 ug/mL Rapamycin for the indicated time, fixed with 2.2% formaldehyde for 15 min, and quenched with 150mM Glycine for 10 min. For longer incubation time with Rapamycin, yeast cultures are appropriately diluted with fresh YPAD medium and Rapamycin to maintain cells' exponential growth phase. Yeast Rpb1 Chromatin immunoprecipitation and following library preparation were performed as described previously (D'Urso et al., 2016), except for use of anti-Rpb1 CTD antibody 8WG16 and 2.5% spike-in human HCT116 chromatin. Reads were aligned to a concatenated genome of sacCer3 and hg38 assembly.

PRO-seq—Library preparation for PRO-seq in human cells with fly spike-in normalization and data analysis were performed as described previously (Aoi et al., 2020) with minor modification. Briefly, ~1 millon human DLD-1 nuclei were mixed with spike-in *Drosophila* S2 nuclei, then used for the nuclear run-on assays as described in qPRO-seq protocol (Judd et al., 2020). Following adaptor ligation with VRA3 and VRA5, reverse transcription and DNA library amplification, DNA libraries were sequenced on NovaSeq 6000 (Illumina). Low-quality bases and adapters from 3' ends of reads were removed using cutadapt 1.14 (Martin, 2011) requiring a read length of 16–36 bp, followed by removal of reads that were derived from ribosomal RNA. The remaining reads were aligned using bowtie 2.2.6 with --very-sensitive option (Langmead and Salzberg, 2012), to a concatenated genome comprised of human hg38 and fly dm6 assemblies. Counts of the 5' end of aligned reads with MAPQ ≥ 30 were normalized to total reads aligned to the spike-in genome.

TT-seq with pulse-chase RNA labeling—~20 million cells were treated with 250 nM NVP-2 for 1 h, followed by nascent RNA labeling with 500 μM 4-thiouridin (4sU) (Sigma # T4509) for 15 min. TT-seq library preparation was performed as described previously (Rosencrance et al., 2020; Schwalb et al., 2016). Briefly, following 4sU labeling, total RNA was extracted using TRIzol (ThermoFisher # 15596026). Spike-in was not included, since this experiment was shown to quantify elongation rates and not Pol II levels, which were already shown by the ChIP-seq and PRO-seq. Total RNA was fragmented using Magnesium RNA Fragmentation Module (NEB #E6150S), followed by biotinylation of 4sU using Biotin-XX-MTSEA (Biotium #90066) in 20% DMF. Biotinylated RNA was enriched using Dynabeads MyOne Streptavidin C1 (ThermoFisher #65001), followed by reduction of disulfide bonds in 100 mM DTT for RNA elution. DNA libraries that were prepared from the enriched RNA fragments were sequenced on NovaSeq 6000. Low-quality bases were

removed from 3' ends using cutadapt 1.14 (Martin, 2011). Reads were aligned to human hg38 genome assembly with Ensembl annotation data release 103 using STAR 2.7.5 (Dobin et al., 2013). Counts of reads with primary alignments and MAPQ ≥ 7 were normalized to total mapped reads.

Visualization of protein structures—To visualize structural model, the following available data are used: Pol II with DSIF (PDB: 5XON) (Ehara et al., 2017), Pol II at the initiation step (PDB: 3K7A) (Liu et al., 2010), Pol II on the nucleosome (PDB: 6A5P, 6A5T) (Kujirai et al., 2018), NELF-Pol II complex (PDB: 6GML) (Vos et al., 2018), VCP (PDB: 5FTK) (Banerjee et al., 2016), proteasome (PDB: 4CR2) (Unverdorben et al., 2014), CDK9 (PDB: 4EC9) (Baumli et al., 2012).

QUANTIFICATION AND STATISTICAL ANALYSIS

Protein identification from MS data—Protein Tandem MS data was queried for protein identification and label-free quantification against Swiss-Prot *Homo Sapiens* database using MaxQuant v1.6.0.16 (Cox et al., 2014). The following modifications were set as search parameters: peptide mass tolerance at 6 ppm, trypsin digestion cleavage after K or R (except when followed by P), 2 allowed missed cleavage site, carbamidomethylated cystein (static modification), and oxidized methionine, protein N-term acetylation (variable modification). Search results were validated with peptide and protein FDR both at 0.01. MaxQuant raw data are available on ProteomeXchange.

Statistical analysis of protein abundance—MaxQuant quantification data were normalized to Pol II levels using MSstats v4.0.0 (Choi et al., 2014) with GlobalStandards method using RPB1, RPB2, RPB3, RPB4, RPB5 as standard proteins. Run summarization from subplot model was performed with Tukey's median polish robust estimation. Imputation of missing values was carried out using QRILC method in imputeLCMD v2.0 (Lazar, 2015). Moderated t-test with 3 biological replicates was carried out using limma v3.48.0 (Ritchie et al., 2015). Proteins with > 2.5 fold change and observed p-value < 0.05 were shown in Table S1.

Analysis of sequencing signal data—Meta plots of mean signal and heat maps of signal at the indicated regions were generated using deepTools 3.1.1 (Ramírez et al., 2016). Protein coding genes and promoter-proximal pause sites in DLD-1 cell lines were chosen as described previously (Aoi et al., 2020). For transcript annotation in *S. cerevisiae*, observed TSSs previously identified from PRO-cap data (Booth et al., 2016) were used to generate meta-gene heat maps.

Estimation of Pol II elongation velocity—The meta-gene and single-gene level elongation rate estimates were calculated using DRB/TT-seq script described in (Gregersen et al., 2020). In addition to our TT-seq data set above, we also prepared another set of TT-seq: cells were treated with 250 nM NVP-2 for 0, 30, 60 min, followed by nascent RNA labeling with 500 μM 4-thiouridin (4sU) (Sigma # T4509) for 10 min. TT-seq libraries were prepared as described above. For estimation of elongation rates, we used bigwig files that were generated by alignment using bowtie 2.2.6. For the meta-gene level analysis,

we selected n=226 non-overlapping, protein coding genes longer than 240kb, which map to standard chromosomes. Single-gene estimates were calculated for these genes which passed additional requirements of minimum 100 RPM, having no missing values, and which wave advanced with time in the control condition (n=69 genes). Smoothing spline fitting parameter (spar) was set to 0.95 to ensure a robust peak detection, the observation window spanned over 225kb, from 5kb downstream of TSS (to mitigate the initiation artifact) to 230kb downstream of TSS. For the TT-seq time series data, in our case 30min and 60min, DRB/TT-seq R pipeline calls RNAPII transcription wave peak positions and estimates elongation rates (kb/min) by fitting a linear model. The slope coefficient of the model is interpreted as the elongation rate estimate. For statistical analysis, pairwise comparisons Mann Whitney U Test (Wilcoxon Rank Sum Test) was used.

Supplementary Material

Refer to Web version on PubMed Central for supplementary material.

Acknowledgments

We are grateful to Dr. Edwin Smith for discussions and critical reading of the manuscript. We thank the Shilatifard lab members for helpful discussions and supports, and B. Monroe for illustrations. We thank M. Kanemaki, A. Holland, I. Cheeseman, D. Foltz, B. Zheng for providing reagents. We thank K. Eagan for advice on TT-seq. Y.A. was supported by the JSPS Research Fellowship for Young Scientists and the Uehara Memorial Foundation Research Fellowship. Proteomics analysis was performed by the Northwestern Proteomics Core Facility, supported by NCI CCSG P30 CA060553 awarded to the Robert H Lurie Comprehensive Cancer Center, instrumentation award (S10OD025194) from NIH Office of Director, and the National Resource for Translational and Developmental Proteomics supported by P41 GM108569. The study is supported by funding through generous support by the National Cancer Institute grant R01CA214035–19 to A.S.

References

Anindya R, Aygün O, and Svejstrup JQ (2007). Damage-induced ubiquitylation of human RNA polymerase II by the ubiquitin ligase Nedd4, but not Cockayne syndrome proteins or BRCA1. Molecular Cell 28, 386–397. [PubMed: 17996703]

Aoi Y, Smith ER, Shah AP, Rendleman EJ, Marshall SA, Woodfin AR, Chen FX, Shiekhattar R, and Shilatifard A. (2020). NELF Regulates a Promoter-Proximal Step Distinct from RNA Pol II Pause-Release. Molecular Cell 78, 261–274.e265. [PubMed: 32155413]

Banerjee S, Bartesaghi A, Merk A, Rao P, Bulfer SL, Yan Y, Green N, Mroczkowski B, Neitz RJ, Wipf P., et al. (2016). 2.3 Å resolution cryo-EM structure of human p97 and mechanism of allosteric inhibition. Science 351, 871–875. [PubMed: 26822609]

Baumli S, Hole AJ, Wang L-Z, Noble MEM, and Endicott JA (2012). The CDK9 tail determines the reaction pathway of positive transcription elongation factor b. Structure 20, 1788–1795. [PubMed: 22959624]

Booth GT, Wang IX, Wang IX, Cheung VG, Cheung VG, and Lis JT (2016). Divergence of a conserved elongation factor and transcription regulation in budding and fission yeast. Genome Res. 26, 799–811. [PubMed: 27197211]

Brown SA, Imbalzano AN, and Kingston RE (1996). Activator-dependent regulation of transcriptional pausing on nucleosomal templates. Genes & Development 10, 1479–1490. [PubMed: 8666232]

Chen FX, Smith ER, and Shilatifard A. (2018). Born to run: control of transcription elongation by RNA polymerase II. Nat Rev Mol Cell Biol 19, 464–478. [PubMed: 29740129]

Chen FX, Xie P, Collings CK, Cao K, Aoi Y, Marshall SA, Rendleman EJ, Ugarenko M, Ozark PA, Zhang A., et al. (2017). PAF1 regulation of promoter-proximal pause release via enhancer activation. Science 357, 1294–1298. [PubMed: 28860207]

Chen H-Y, and Chen R-H (2016). Cullin 3 Ubiquitin Ligases in Cancer Biology: Functions and Therapeutic Implications. Front Oncol 6, 113. [PubMed: 27200299]

Choi M, Chang C-Y, Clough T, Broudy D, Killeen T, MacLean B, and Vitek O. (2014). MSstats: an R package for statistical analysis of quantitative mass spectrometry-based proteomic experiments. Bioinformatics 30, 2524–2526. [PubMed: 24794931]

Cortazar MA, Sheridan RM, Erickson B, Fong N, Glover-Cutter K, Brannan K, and Bentley DL (2019). Control of RNA Pol II Speed by PNUTS-PP1 and Spt5 Dephosphorylation Facilitates Termination by a "Sitting Duck Torpedo" Mechanism. Molecular Cell 76, 896–908.e4. [PubMed: 31677974]

Cox J, Hein MY, Luber CA, Paron I, Nagaraj N, and Mann M. (2014). Accurate proteome-wide label-free quantification by delayed normalization and maximal peptide ratio extraction, termed MaxLFQ. Mol. Cell Proteomics 13, 2513–2526. [PubMed: 24942700]

D'Urso A, Takahashi Y-H, Xiong B, Marone J, Coukos R, Randise-Hinchliff C, Wang J-P, Shilatifard A, and Brickner JH (2016). Set1/COMPASS and Mediator are repurposed to promote epigenetic transcriptional memory. Elife 5, 111.

Decker TM (2020). Mechanisms of Transcription Elongation Factor DSIF (Spt4-Spt5). J. Mol. Biol 55, 166657.

Diamant G, Bahat A, and Dikstein R. (2016). The elongation factor Spt5 facilitates transcription initiation for rapid induction of inflammatory-response genes. Nature Communications 7, 11547.

Doamekpor SK, Sanchez AM, Schwer B, Shuman S, and Lima CD (2014). How an mRNA capping enzyme reads distinct RNA polymerase II and Spt5 CTD phosphorylation codes. Genes & Development 28, 1323–1336. [PubMed: 24939935]

Dobin A, Davis CA, Schlesinger F, Drenkow J, Zaleski C, Jha S, Batut P, Chaisson M, and Gingeras TR (2013). STAR: ultrafast universal RNA-seq aligner. Bioinformatics 29, 15–21. [PubMed: 23104886]

Dubiel W, Dubiel D, Wolf DA, and Naumann M. (2018). Cullin 3-Based Ubiquitin Ligases as Master Regulators of Mammalian Cell Differentiation. Trends Biochem. Sci 43, 95–107. [PubMed: 29249570]

Ehara H, Kujirai T, Fujino Y, Shirouzu M, Kurumizaka H, and Sekine S-I (2019). Structural insight into nucleosome transcription by RNA polymerase II with elongation factors. Science 363, 744–747. [PubMed: 30733384]

Ehara H, Yokoyama T, Shigematsu H, Yokoyama S, Shirouzu M, and Sekine S-I (2017). Structure of the complete elongation complex of RNA polymerase II with basal factors. Science eaan8552–eaan8558.

Fitz J, Neumann T, and Pavri R. (2018). Regulation of RNA polymerase II processivity by Spt5 is restricted to a narrow window during elongation. Embo J 37.

Gregersen LH, and Svejstrup JQ (2018). The Cellular Response to Transcription- Blocking DNA Damage. Trends Biochem. Sci 43, 327–341. [PubMed: 29699641]

Gregersen LH, Mitter R, and Svejstrup JQ (2020). Using TTchem-seq for profiling nascent transcription and measuring transcript elongation. Nat Protoc 15, 604–627. [PubMed: 31915390]

Guo S, Yamaguchi Y, Schilbach S, Wada T, Lee J, Goddard A, French D, Handa H, and Rosenthal A. (2000). A regulator of transcriptional elongation controls vertebrate neuronal development. Nature 408, 366–369. [PubMed: 11099044]

Haruki H, Nishikawa J, and Laemmli UK (2008). The anchor-away technique: rapid, conditional establishment of yeast mutant phenotypes. Molecular Cell 31, 925–932. [PubMed: 18922474]

He J, Zhu Q, Wani G, and Wani AA (2017). UV-induced proteolysis of RNA polymerase II is mediated by VCP/p97 segregase and timely orchestration by Cockayne syndrome B protein. Oncotarget 8, 11004–11019. [PubMed: 28036256]

Holland AJ, Fachinetti D, Han JS, and Cleveland DW (2012). Inducible, reversible system for the rapid and complete degradation of proteins in mammalian cells. Proceedings of the National Academy of Sciences 109, E3350–E3357.

Hou L, Wang Y, Liu Y, Zhang N, Shamovsky I, Nudler E, Tian B, and Dynlacht BD (2019). Paf1C regulates RNA polymerase II progression by modulating elongation rate. Proc. Natl. Acad. Sci. U.S.a 116, 14583–14592. [PubMed: 31249142]

Huang K-L, Jee D, Stein CB, Elrod ND, Henriques T, Mascibroda LG, Baillat D, Russell WK, Adelman K, and Wagner EJ (2020). Integrator Recruits Protein Phosphatase 2A to Prevent Pause Release and Facilitate Transcription Termination. Molecular Cell 80, 345–358.e349. [PubMed: 32966759]

Jang MK, Mochizuki K, Zhou M, Jeong H-S, Brady JN, and Ozato K. (2005). The Bromodomain Protein Brd4 Is a Positive Regulatory Component of P-TEFb and Stimulates RNA Polymerase II-Dependent Transcription. Molecular Cell 19, 523–534. [PubMed: 16109376]

Jonkers I, Kwak H, and Lis JT (2014). Genome-wide dynamics of Pol II elongation and its interplay with promoter proximal pausing, chromatin, and exons. Elife 3, 720–725.

Judd J, Wojenski LA, Wainman LM, Tippens ND, Rice EJ, Dziubek A, Villafano GJ, Wissink EM, Versluis P, Bagepalli L., et al. (2020). A rapid, sensitive, scalable method for Precision Run-On sequencing (PRO-seq). bioRxiv 1–34.

Komori T, Inukai N, Yamada T, Yamaguchi Y, and Handa H. (2009). Role of human transcription elongation factor DSIF in the suppression of senescence and apoptosis. Genes to Cells 14, 343–354. [PubMed: 19210550]

Kujirai T, Ehara H, Fujino Y, Shirouzu M, Sekine S-I, and Kurumizaka H. (2018). Structural basis of the nucleosome transition during RNA polymerase II passage. Science 362, 595–598. [PubMed: 30287617]

Kwak H, Fuda NJ, Core LJ, and Lis JT (2013). Precise maps of RNA polymerase reveal how promoters direct initiation and pausing. Science 339, 950–953. [PubMed: 23430654]

Langmead B, and Salzberg SL (2012). Fast gapped-read alignment with Bowtie 2. Nat Meth 9, 357–359.

Lazar C. (2015). imputeLCMD: a collection of methods for left-censored missing data imputation. R Package, Version 2.

Li S, Prasanna X, Salo VT, Vattulainen I, and Ikonen E. (2019). An efficient auxin-inducible degron system with low basal degradation in human cells. Nat Meth 16, 866–869.

Liang K, Smith ER, Aoi Y, Stoltz KL, Katagi H, Woodfin AR, Rendleman EJ, Marshall SA, Murray DC, Wang L., et al. (2018). Targeting Processive Transcription Elongation via SEC Disruption for MYC-Induced Cancer Therapy. Cell 175, 766–779.e17. [PubMed: 30340042]

Lin C, Smith ER, Takahashi H, Lai KC, Martin-Brown S, Florens L, Washburn MP, Conaway JW, Conaway RC, and Shilatifard A. (2010). AFF4, a component of the ELL/P-TEFb elongation complex and a shared subunit of MLL chimeras, can link transcription elongation to leukemia. Molecular Cell 37, 429–437. [PubMed: 20159561]

Liu X, Bushnell DA, Wang D, Calero G, and Kornberg RD (2010). Structure of an RNA polymerase II-TFIIB complex and the transcription initiation mechanism. Science 327, 206–209. [PubMed: 19965383]

Magnaghi P, D'Alessio R, Valsasina B, Avanzi N, Rizzi S, Asa D, Gasparri F, Cozzi L, Cucchi U, Orrenius C., et al. (2013). Covalent and allosteric inhibitors of the ATPase VCP/p97 induce cancer cell death. Nature Chemical Biology 9, 548–556. [PubMed: 23892893]

Martin M. (2011). Cutadapt removes adapter sequences from highthroughput sequencing reads. EMBnet 17, 10–12.

Mylonas C, Lee C, Auld AL, Cisse II, and Boyer LA (2021). A dual role for H2A.Z.1 in modulating the dynamics of RNA polymerase II initiation and elongation. Nat. Struct. Mol. Biol 1–36.

Narita T, Yamaguchi Y, Yano K, Sugimoto S, Chanarat S, Wada T, Kim D-K, Hasegawa J, Omori M, Inukai N., et al. (2003). Human transcription elongation factor NELF: identification of novel subunits and reconstitution of the functionally active complex. Molecular and Cellular Biology 23, 1863–1873. [PubMed: 12612062]

Natsume T, Kiyomitsu T, Saga Y, and Kanemaki MT (2016). Rapid Protein Depletion in Human Cells by Auxin-Inducible Degron Tagging with Short Homology Donors. Cell Rep 15, 210–218. [PubMed: 27052166]

Olson CM, Jiang B, Erb MA, Liang Y, Doctor ZM, Zhang Z, Zhang T, Kwiatkowski N, Boukhali M, Green JL, et al. (2018). Pharmacological perturbation of CDK9 using selective CDK9 inhibition or degradation. Nature Chemical Biology 14, 163–170. [PubMed: 29251720]

Parua PK, Booth GT, Sansó M, Benjamin B, Tanny JC, Lis JT, and Fisher RP (2018). A Cdk9-PP1 switch regulates the elongation-termination transition of RNA polymerase II. Nature 558, 460–464. [PubMed: 29899453]

Pavri R, Gazumyan A, Jankovic M, Di Virgilio M, Klein I, Ansarah-Sobrinho C, Resch W, Yamane A, San-Martin BR, Barreto V., et al. (2010). Activation-Induced Cytidine Deaminase Targets DNA at Sites of RNA Polymerase II Stalling by Interaction with Spt5. Cell 143, 122–133. [PubMed: 20887897]

Rahl PB, Lin CY, Seila AC, Flynn RA, McCuine S, Burge CB, Sharp PA, and Young RA (2010). c-Myc Regulates Transcriptional Pause Release. Cell 141, 432–445. [PubMed: 20434984]

Ramírez F, Ryan DP, Grüning B, Bhardwaj V, Kilpert F, Richter AS, Heyne S, Dündar F, and Manke T. (2016). deepTools2: a next generation web server for deep-sequencing data analysis. Nucleic Acids Res. 44, W160–W165. [PubMed: 27079975]

Ritchie ME, Phipson B, Wu D, Hu Y, Law CW, Shi W, and Smyth GK (2015). limma powers differential expression analyses for RNA-sequencing and microarray studies. Nucleic Acids Res. 43, e47–e47. [PubMed: 25605792]

Rosencrance CD, Ammouri HN, Yu Q, Ge T, Rendleman EJ, Marshall SA, and Eagen KP (2020). Chromatin Hyperacetylation Impacts Chromosome Folding by Forming a Nuclear Subcompartment. Molecular Cell 78, 112–126.e112. [PubMed: 32243828]

Sansó M, Levin RS, Lipp JJ, Wang VY-F, Greifenberg AK, Quezada EM, Ali A, Ghosh A, Larochelle S, Rana TM, et al. (2016). P-TEFb regulation of transcription termination factor Xrn2 revealed by a chemical genetic screen for Cdk9 substrates. Genes & Development 30, 117–131. [PubMed: 26728557]

Schwalb B, Schwalb B, Michel M, Zacher B, Frühauf K, Demel C, Demel C, Tresch A, Gagneur J, and Cramer P. (2016). TT-seq maps the human transient transcriptome. Science 352, 1225–1228. [PubMed: 27257258]

Shetty A, Kallgren SP, Demel C, Maier KC, Spatt D, Alver BH, Cramer P, Park PJ, and Winston F. (2017). Spt5 Plays Vital Roles in the Control of Sense and Antisense Transcription Elongation. Molecular Cell 66, 77–88.e5. [PubMed: 28366642]

Steinmetz EJ, Warren CL, Kuehner JN, Panbehi B, Ansari AZ, and Brow DA (2006). Genome-wide distribution of yeast RNA polymerase II and its control by Sen1 helicase. Molecular Cell 24, 735–746. [PubMed: 17157256]

Titov DV, Gilman B, He Q-L, Bhat S, Low W-K, Dang Y, Smeaton M, Demain AL, Miller PS, Kugel JF, et al. (2011). XPB, a subunit of TFIIH, is a target of the natural product triptolide. Nature Chemical Biology 7, 182–188. [PubMed: 21278739]

Tufegdžić Vidaković A, Mitter R, Kelly GP, Neumann M, Harreman M, Rodríguez-Martínez M, Herlihy A, Weems JC, Boeing S, Encheva V., et al. (2020). Regulation of the RNAPII Pool Is Integral to the DNA Damage Response. Cell 180, 1245–1261.e21. [PubMed: 32142654]

Unverdorben P, Beck F, Śledź P, Schweitzer A, Pfeifer G, Plitzko JM, Baumeister W, and Förster F. (2014). Deep classification of a large cryo-EM dataset defines the conformational landscape of the 26S proteasome. Proc. Natl. Acad. Sci. U.S.a 111, 5544–5549. [PubMed: 24706844]

van den Boom J, and Meyer H. (2018). VCP/p97-Mediated Unfolding as a Principle in Protein Homeostasis and Signaling. Molecular Cell 69, 182–194. [PubMed: 29153394]

Vispé S, DeVries L, Créancier L, Besse J, Bréand S, Hobson DJ, Svejstrup JQ, Annereau J-P, Cussac D, Dumontet C., et al. (2009). Triptolide is an inhibitor of RNA polymerase I and II-dependent transcription leading predominantly to down-regulation of short-lived mRNA. Mol. Cancer Ther 8, 2780–2790. [PubMed: 19808979]

Vos SM, Farnung L, Urlaub H, and Cramer P. (2018). Structure of paused transcription complex Pol II-DSIF-NELF. Nature 560, 601–606. [PubMed: 30135580]

Wada T, Wada T, Takagi T, Takagi T, Yamaguchi Y, Yamaguchi Y, Ferdous A, Imai T, Hirose S, Sugimoto S., et al. (1998). DSIF, a novel transcription elongation factor that regulates RNA polymerase II processivity, is composed of human Spt4 and Spt5 homologs. Genes & Development 12, 343–356. [PubMed: 9450929]

Winter GE, Mayer A, Buckley DL, Erb MA, Roderick JE, Vittori S, Reyes JM, di Iulio J, Souza A, Ott CJ, et al. (2017). BET Bromodomain Proteins Function as Master Transcription Elongation Factors Independent of CDK9 Recruitment. Molecular Cell 67, 5–18.e19. [PubMed: 28673542]

Xu J, Lahiri I, Wang W, Wier A, Cianfrocco MA, Chong J, Hare AA, Dervan PB, DiMaio F, Leschziner AE, et al. (2017). Structural basis for the initiation of eukaryotic transcription-coupled DNA repair. Nature 551, 653–657. [PubMed: 29168508]

Yamada T, Yamaguchi Y, Inukai N, Okamoto S, Mura T, and Handa H. (2006). P-TEFb-Mediated Phosphorylation of hSpt5 C-Terminal Repeats Is Critical for Processive Transcription Elongation. Molecular Cell 21, 227–237. [PubMed: 16427012]

Yamaguchi Y, Yamaguchi Y, Takagi T, Takagi T, Wada T, Wada T, Yano K, Yano K, Furuya A, Furuya A., et al. (1999). NELF, a multisubunit complex containing RD, cooperates with DSIF to repress RNA polymerase II elongation. Cell 97, 41–51. [PubMed: 10199401]

Yamaguchi Y, Inukai N, Narita T, Wada T, and Handa H. (2002). Evidence that negative elongation factor represses transcription elongation through binding to a DRB sensitivity-inducing factor/RNA polymerase II complex and RNA. Molecular and Cellular Biology 22, 2918–2927. [PubMed: 11940650]

Yang Z, Yik JHN, Chen R, He N, Jang MK, Ozato K, and Zhou Q. (2005). Recruitment of P-TEFb for Stimulation of Transcriptional Elongation by the Bromodomain Protein Brd4. Molecular Cell 19, 535–545. [PubMed: 16109377]

Yasukawa T, Kamura T, Kitajima S, Conaway RC, Conaway JW, and Aso T. (2008). Mammalian Elongin A complex mediates DNA-damage-induced ubiquitylation and degradation of Rpb1. Embo J 27, 3256–3266. [PubMed: 19037258]

Zheng B, Aoi Y, Shah AP, Iwanaszko M, Das S, Rendleman EJ, Zha D, Khan N, Smith ER, and Shilatifard A. (2021). Acute perturbation strategies in interrogating RNA polymerase II elongation factor function in gene expression. Genes & Development 35, 273–285. [PubMed: 33446572]

Žumer K, Maier KC, Farnung L, Jaeger MG, Rus P, Winter G, and Cramer P. (2021). Two distinct mechanisms of RNA polymerase II elongation stimulation in vivo. Molecular Cell.

Highlights

- Acute depletion of SPT5 triggers degradation of Pol II subunit RPB1
- E3 ligase CUL3 is recruited to Pol II upon SPT5 loss, leading to RPB1 degradation
- VCP unfoldase inhibition dissects SPT5's roles in Pol II elongation and stability
- SPT5 licenses promoter-proximal Pol II release by regulating Pol II stability

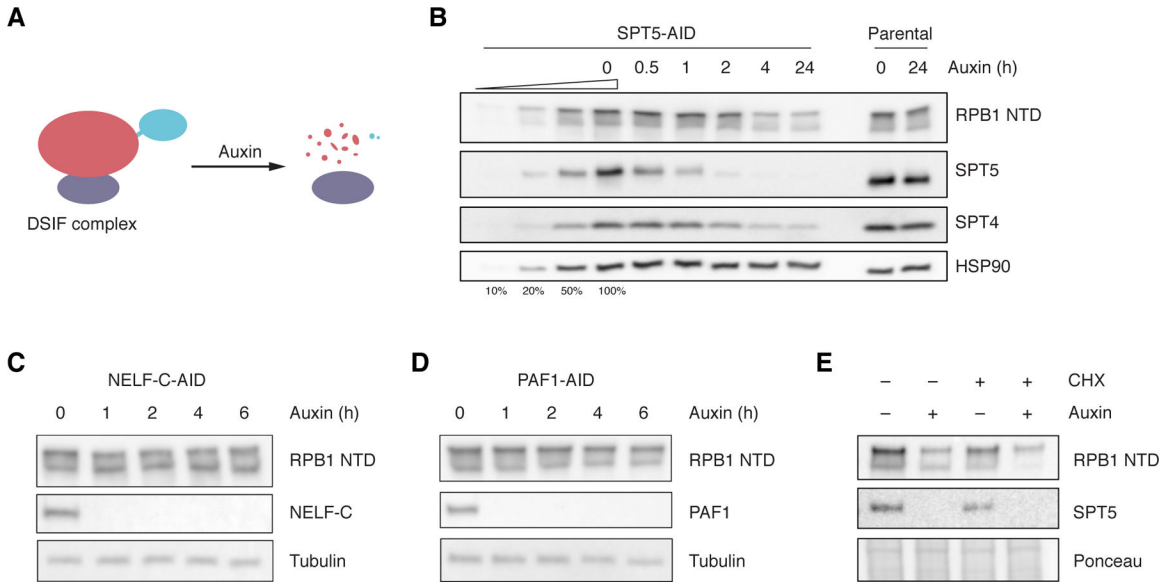

Figure 1. Rapid SPT5 depletion leads to RPB1 degradation.

(A) Schematic of auxin-inducible degradation of SPT5-AID protein.

(B) Western blots of the indicated proteins in whole-cell lysates of SPT5-AID or parental DLD-1 cells. Cells were treated with 500 μM auxin for the indicated time. SPT5-AID was depleted within 2 h of auxin treatment, at which time the RPB1 loss was observed. HSP90 serves as a loading control. A triangle indicates increasing amounts of lysates. RPB1 NTD antibody D8L4Y was used to detect total RPB1 levels.

(C, D) Western blots in NELF-C-AID (C) or PAF1-AID (D) cells treated with auxin as in (B). RPB1 levels were stable upon depletion of NELF or PAF1. RPB1 NTD antibody D8L4Y was used to detect total RPB1 levels.

(E) Western blots in SPT5-AID cells treated with translation inhibitor cycloheximide (CHX) for 4 h, followed by treatment with 500 μM auxin for 3 h. RPB1 loss was still observed when protein synthesis was blocked, indicating RPB1 degradation upon SPT5 depletion. RPB1 NTD antibody D8L4Y was used to detect total RPB1 levels. See also Figure S1.

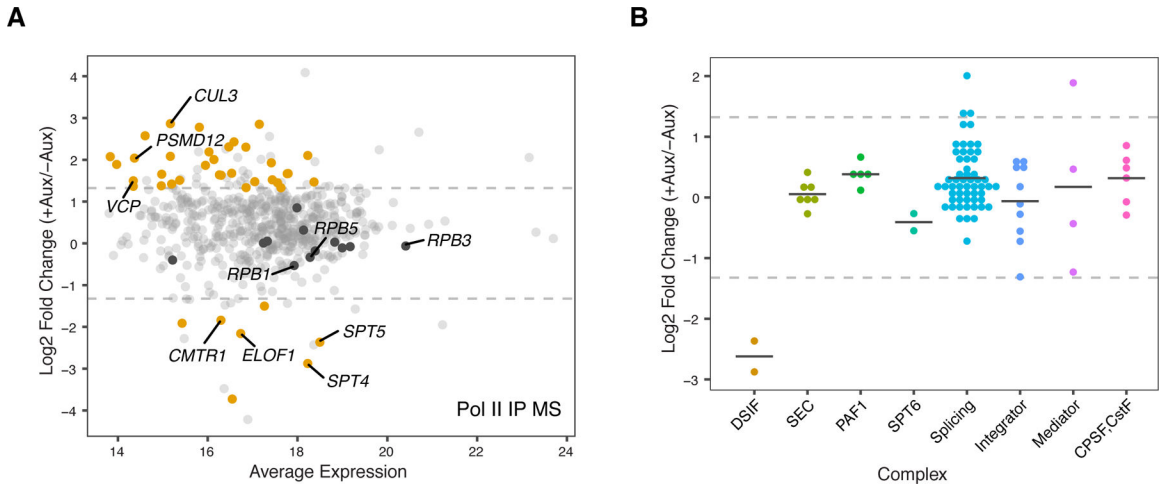

Figure 2. CUL3, VCP and PSMD12 are recruited to Pol II upon SPT5 depletion.

(A) MA plot showing mass spectrometric data of Pol II immunoprecipitation from 3 independent experiments. Proteins with > 2.5-fold change and p-value < 0.05 are shown in orange. Pol II subunits are shown in dark gray. See also Figure S2 and Table S1.

(B) Log2 fold change of Pol II-associated complexes. Each dot indicates a subunit of each complex that was detected in our proteomics data. Dashed lines indicate 2.5-fold change.

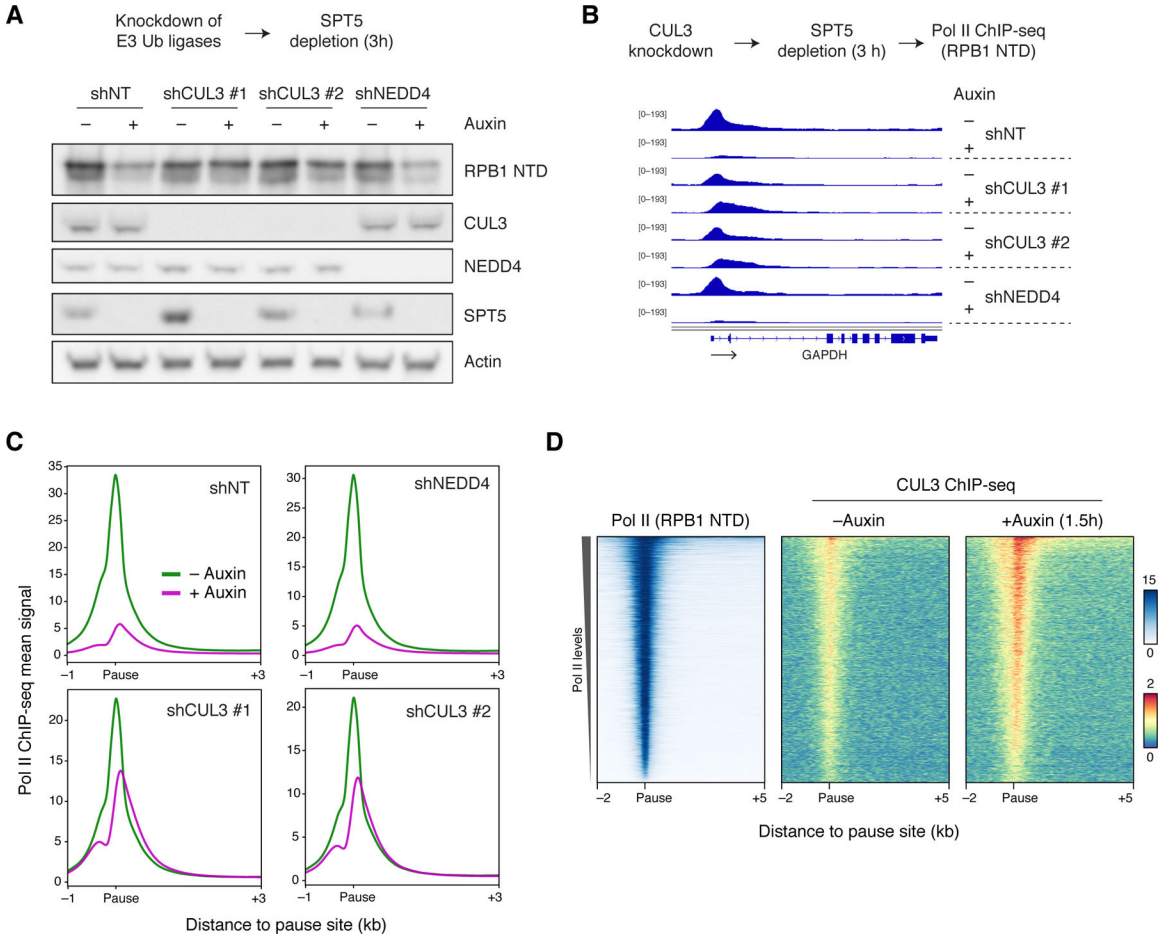

Figure 3. E3 ligase CUL3, but not NEDD4, is required for RPB1 degradation after SPT5 depletion.

(A) Western blots of the indicated proteins in SPT5-AID^7 whole-cell lysates. Cells were treated with shRNA against CUL3 or NEDD4, followed by treatment with 500 μM auxin for 3 h. RPB1 NTD antibody D8L4Y was used to detect total RPB1 levels.

(B) Representative track showing Pol II ChIP-seq signal in SPT5-AID^7 cells. Cells were treated as in (A). RPB1 NTD antibody D8L4Y was used to detect total RPB1 signal.

(C) Meta plots of Pol II ChIP-seq in SPT5-AID^7 cells treated as in (A). Signal is centered on promoter-proximal pause site. N = 6,524.

(D) Heat map of ChIP-seq signal for Pol II and CUL3. Rows are sorted by Pol II occupancy levels. SPT5-AID cells were treated with or without 500 μM auxin for 1.5 h. Note that auxin treatment for 1.5 h leads to a limited degradation of RPB1. N = 6,524. See also Figure S3.

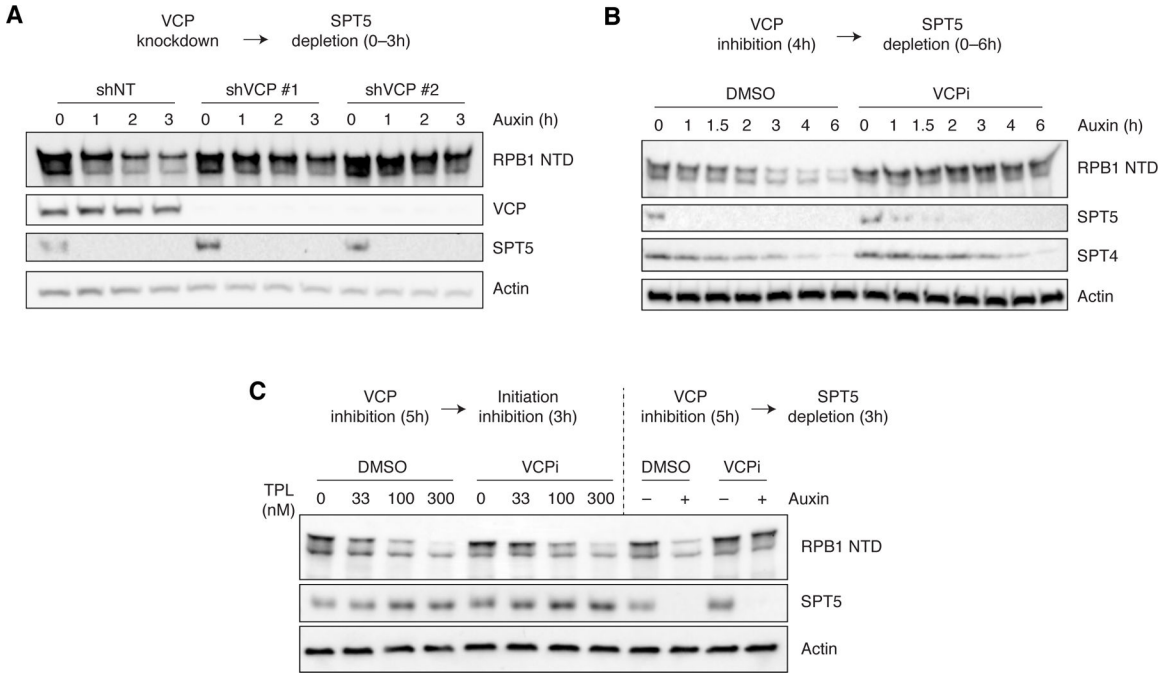

Figure 4. Unfoldase VCP is required for RPB1 degradation induced by SPT5 depletion in human and yeast.

(A) VCP knockdown rescued RPB1 degradation. SPT5-AID cells were treated with the indicated shRNA, followed by treatment with 500 μM auxin for the indicated time. NT, non-targeting. Actin serves as a loading control. RPB1 NTD antibody D8L4Y was used to detect total RPB1 levels.

(B) Pharmacological inhibition of VCP rescued RPB1 degradation. SPT5-AID cells were treated with 2.5 μM VCP inhibitor NMS-873 (VCPi) for 4 h, followed by treatment with 500 μM auxin for the indicated time. Actin serves as a loading control. RPB1 NTD antibody D8L4Y was used to detect total RPB1 levels.

(C) Inhibition of transcription initiation led to VCP-independent RPB1 degradation. SPT5-AID cells were treated with 2.5 μM NMS-873 (VCPi) for 5 h, followed by treatment with a range of dosage of initiation inhibitor triptolide (TPL) for 3 h. As a control, cells were treated with 500 μM auxin instead of TPL. RPB1 NTD antibody D8L4Y was used to detect total RPB1 levels. See also Figure S4.

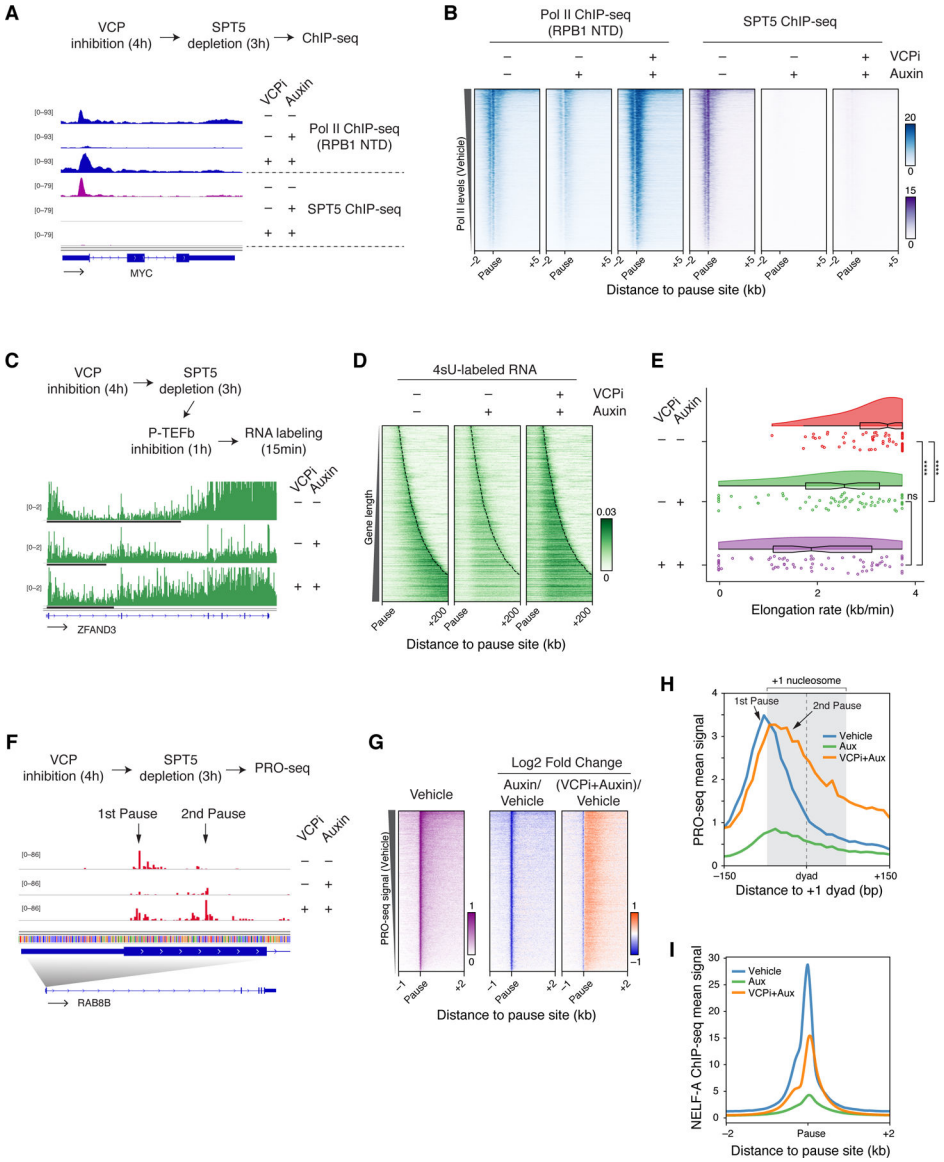

Figure 5. SPT5 depletion results in destabilization of Pol II during early elongation.

(A) Representative genome browser track example showing ChIP-seq signal for Pol II (blue) and SPT5 (purple) in SPT5-AID cells. Cells were treated with 2.5 μM NMS-873 (VCPi) for 4 h, followed by treatment with 500 μM auxin for 3 h. RPB1 NTD antibody D8L4Y was used to detect total RPB1 signal.

(B) Heat map of ChIP-seq for Pol II and SPT5. SPT5-AID cells were treated as in (A). Rows are sorted by Pol II occupancy levels in the vehicle (untreated) sample. N = 6,524.

(C) Pulse-chase nascent RNA labeling assay. SPT5-AID cells were treated with 2.5 μM NMS-873 (VCPi) for 4 h, then 500 μM auxin for 3 h. After that, cells were treated with 250 nM P-TEFb inhibitor NVP-2 for 1 h, followed by nascent RNA labeling with 500 μM 4sU for 15 min. Representative tracks of TT-seq signal (labeled nascent RNA) is shown. Inhibition of P-TEFb blocks pause escape but not elongation of Pol II that has already

escaped (Jonkers et al., 2014). Horizontal black lines along tracks indicate the distance that Pol II travels for 1 h.

(D) Heat maps of TT-seq signal in SPT5-AID cells treated as in (C). Rows are sorted by gene length. Curved lines in heat maps indicate transcription end site (TES). N = 2,386 genes with length of ≥50 kb.

(E) Rain cloud plot showing single-gene level estimates of Pol II elongation rate. N = 69 genes with length of > 240 kb and >100 rpm. **** indicates $p < 3 \times 10^{-7}$ and ns indicates "not significant" (p = 0.058) in Mann Whitney U test.

(F) Representative track showing PRO-seq signal in SPT5-AID cells at promoter-proximal regions. Cells were treated as in (A).

(G) Heat map of PRO-seq signal. The left panel shows PRO-seq signal in the untreated condition (vehicle), and the right 2 panels show log2 fold change relative to vehicle. N = 6,524.

(H) Meta plot of PRO-seq signals in SPT5-AID cells treated as in (A). Signal is centered on the +1 nucleosome dyad. Light gray box indicates the position of the +1 nucleosome (dyad ± 75 bp) as determined by MNase-seq. N = 1,843.

(I) Meta profile of NELF ChIP-seq signal at promoter-proximal regions. SPT5-AID cells were treated as in (A). See also Figure S5.

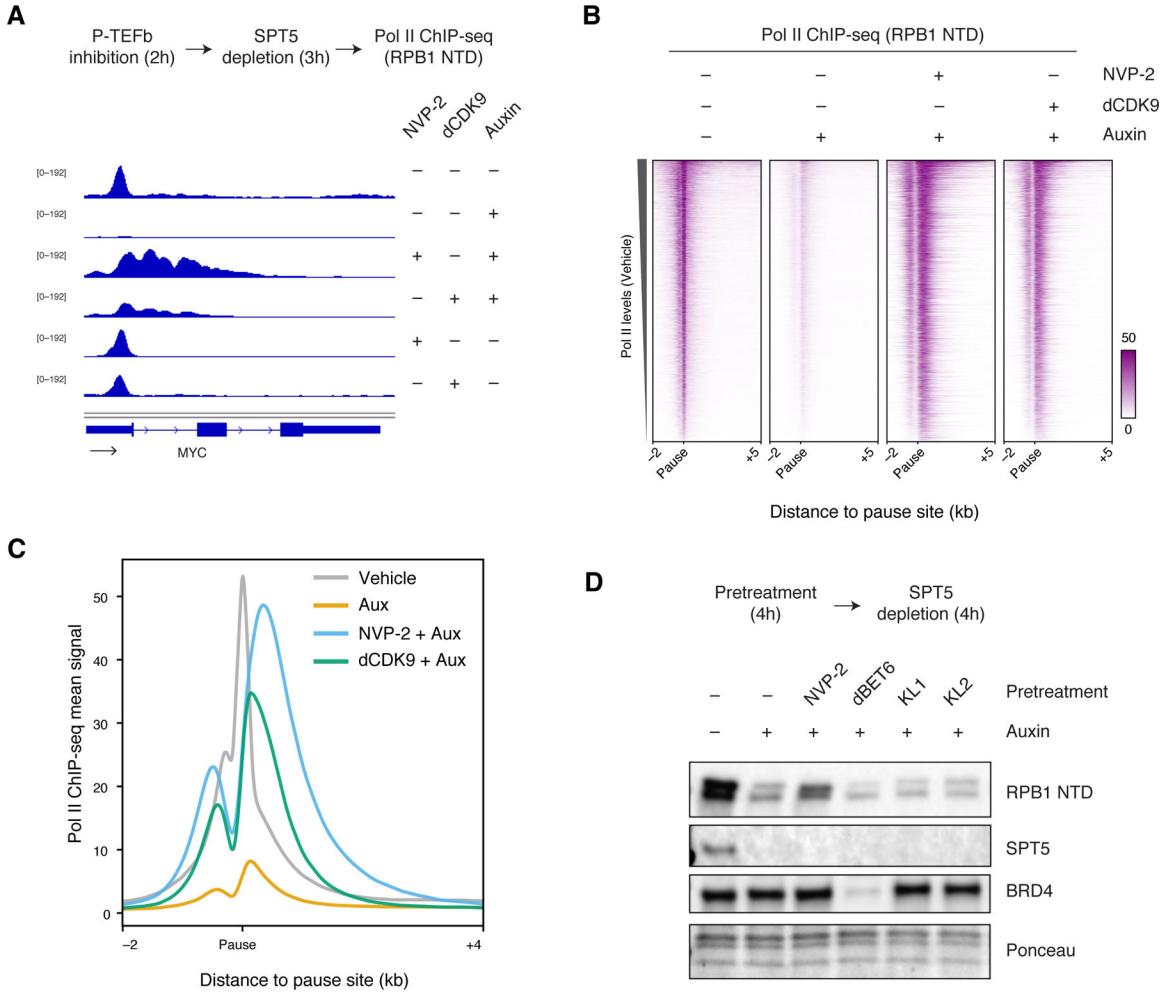

Figure 6. P-TEFb is required for RPB1 degradation induced by SPT5 loss.

(A) Representative track showing Pol II ChIP-seq signal in SPT5-AID cells. Cells were treated with 250 nM P-TEFb inhibitor NVP2 or CDK9 degrader THAL-SNS-032 (dCDK9) for 2 h, followed by treatment with 500 μM auxin for 3 h. RPB1 NTD antibody D8L4Y was used to detect total RPB1 signal.

(B) Heat map of Pol II ChIP-seq in SPT5-AID cells treated as in (A). Rows are sorted by Pol II occupancy levels. N = 6,524.

(C) Meta plot of Pol II ChIP-seq in SPT5-AID cells treated as in (A). Signal is centered on promoter-proximal pause site. N = 6,524.

(D) Western blots of the indicated proteins in SPT5-AID whole-cell lysates. Cells were pretreated with 250 nM NVP-2, 250 nM dBET6, 20 μM KL1 or KL2 for 4 h, followed by 500 μM auxin treatment for 4 h. RPB1 NTD antibody D8L4Y was used to detect total RPB1 levels. See also Figure S6.

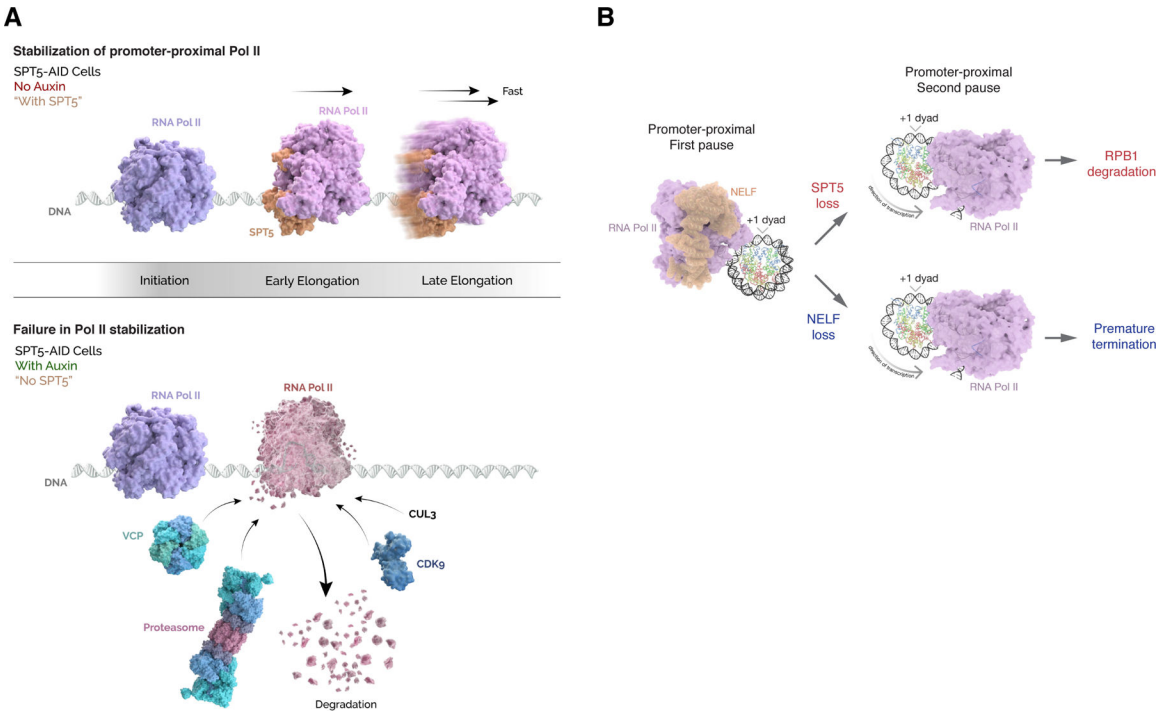

Figure 7. Model: SPT5 stabilizes promoter-proximal Pol II.

(A) SPT5 functions in stabilizing Pol II during the early elongation stage. With SPT5 protein (upper panel), once Pol II is initiated and escapes from the promoter, Pol II undergoes productive elongation until termination. Without SPT5 (lower panel), early elongating Pol II undergoes RPB1 degradation that is mediated by the CUL3 ubiquitin ligase, the VCP unfoldase, and a novel form of P-TEFb component CDK9. Late elongating Pol II without SPT5 can persist in transcription at a slower speed.

(B) A failure in Pol II passage on the +1 nucleosome leads to 2 distinct pathways to eliminate Pol II from chromatin.

KEY RESOURCES TABLE

REAGENT or RESOURCE	SOURCE	IDENTIFIER
Antibodies		
SPT5(for WB and ChiP-seq)	BD Biosciences	Cat# 611107, RRID:AB_398420
SPT4	Cell Signaling Technology	Cat# 64828, RRID:AB_2756442
RPB1 NTD [D8L4Y] (for WB and ChiP-seq for human RPB1)	Cell Signaling Technology	Cat# 14958, RRID:AB_2687876
RPB1 CTD [4H8) (for IP-MS)	Cell Signaling Technology	Cat# 2629, RRID:AB_2167468
RPB1 CTD (for yeast RPB1 WB)	Abcam	Cat# ab26721, RRID:AB_777726
RPB1 CTD [8WG16] (for yeast RPB1 ChiP-seq)	BioLegend	Cat# 664912, RRID:AB_2650945
RPB1 CTD S2P	Millpore	Cat# 04–1571, RRID:AB_10627998
RPB1 CTD S5P	Millpore	Cat# 04–1572, RRlD:AB_10615822
RPB3	Abcam	Cat# ab182150
RPB5	Proteintech	Cat# 15217–1-AP, RRlD:AB_2299932
Tubulin	DSH8	Cat# E7, RRID:AB_528499
HSP90	Santa Cruz Biotechnology	Cat# sc-13119, RRID:AB_675659
Actin	Cell Signaling Technology	Cat# 3700, RRID:AB_2242334
NELF-A	Proteintech	Cat# 10456–1-AP, RRID:AB_2216327
NELF-C	Cell Signaling Technology	Cat# 12265, RRID: AB_2797862
NELF-E	Abcam	Cat# ab170104, RRID:AB_2827280
VCP	Thermo Fisher Scientific	Cat# MA3–004. RRID:AB_2214638
BRD4	Cell Signaling Technology	Cat# 13440, RRID:AB_2687578
H3	Shlatifard Laboratory	N/A
CUL3 (WB and ChiP-seq)	Bethyl	Cat# A301–109A, RRID:AB_873023
CUL5	Bethyl	Cat# A302–173A, RRID:AB_1659801
Chemicals, peptides. and recombinant proteins		
Auxin	Abcam	Cat# ab146403
NMS-873(VCPl)	Sigma-Aidrich	Cat# SML1128
Triptoldo	Tocris	Cat# 3253
NVP-2	MedChemExpress	Cat# HY-12214A
THAL-SNS-032 (dCDK9)	MedChemExpress	Cat# HY-123937
dBET6	Aobious	Cat# AOB37886
KL-1	DC Chemicals	Cat# DC11391
KL-2	DC Chemicals	Cat# DC11392
Rapamycin	ApexBio Technology	Cat# A8167
Benzonase	Sigma	Cat# E1014
Dynabeads Protein G	Invitrogen	Cat# 10004D
4-thiourdin	Sigma	Cat# T4509
Biotin-XX-MTSEA	Bioturn	Cat# 90066
Dynabeads MyOne Streptavidin C1	ThermoFisher	Cat# 65001
Deposited data		

REAGENT or RESOURCE	SOURCE	IDENTIFIER
Sequencing data	This study	GEO: GSE168827
Proteomics data	This study	ProteomaXchange: PXD023997
Experimental models: Cell lines		
OsTIR1 DLD-1	Holland et al, 2012	N/A
SPT5-AID OsTIR1 DLD1 #22–5F-5F	This study	N/A
SPT4-AID OsTlR1 DLD1 #5–1D	This study	N/A
DLD-1	ATCC	Cat# CCL-221
SPT5-AID^{7} AtAFB2 DLD1 #8–9C	This study	N/A
Mouse embryonic fibroblasts	Stem cell technology	Cat# 00325
S2	DGRC	RyBase: FBtc0000006
HCT116	ATCC	Cat# CCL-247
PAF1-AID OsTlR1 DLD1 #5–3G	Chen et al., 2017	N/A
NELF-C-AlD OsTlRI DLD1 #7–10B	Aoi et al., 2020	N/A
NELF-E-AJD OsTlRI DLD1 #20–1B	Aoi et al., 2020	N/A
Experimental models: Organisms/strains		
Yeast Parental anchor strain: HHY168	(Haruki et al., 2008): Euroscarf	Cat# Y40343
Yeast SPT5-FRB-KanMXB (Derivative of HHY168)	This study	N/A
Yeast SPT5-FRB-KanMXB CDC48-FRB-GFP-His3MX6 (Derivative of HHY168)	This study	N/A
Recombinant DNA		
CUL3 GIPZ Lentiviral shRNA #1	Horizon Discovery	Cat# RMS4430–200161789
CUL3 GIPZ Lentiviral shRNA #2	Horizon Discovery	Cat# RHS4430–200258609
NEDD4 GIPZ Lentiviral shRNA	Horizon Discovery	Cat# RHS4430–200286902
VCP GIPZ Lentiviral shRNA #1	Horizon Discovery	Cat# RHS4430–200285689
VCP GIPZ Lentiviral shRNA #2	Horizon Discovery	Cat# RHS4430–200306365
Non-targeting GIPZ Lentiviral shRNA	Horizon Discovery	Cat# RHS4346
SPT5-AID-Neo donor (YNP49)	This study	N/A
SPT5-AID-Hyg donor (YNP50)	This study	N/A
Cas9 for SPT5 (YNP50; gRNA CTTCATCCGACGAAGTCCAC)	This study	N/A
SPT5-AID^{7}-Hyg donor (ANP38)	This study	N/A
SPT5-AID^{7}-Neo donor (ANP39)	This study	N/A
SPT4-AID-Neo donor (ANP68)	This study	N/A
SPT4-AIO-Hyg donor (ANP69)	This study	N/A
Cas9 far SPT4 (ANP71; gRNA GTGCGGGAGCTGAAAAGTCG)	This study	N/A
CUL5 GIPZ Lentiviral shRNA #1	Horizon Discovery	Cat# RHS4430–200181108
CUL5 GIPZ Lentiviral shRNA #2	Horizon Discovery	Cat# RHS4430–200267365
CUL5 GIPZ Lentiviral shRNA #3	Horizon Discovery	Cat# RHS4430–200276360
Software and algorithms		

REAGENT or RESOURCE	SOURCE	IDENTIFIER
bowtie 2.2.6	Langmead and Salzberg,2012	N/A
STAR 2.7.5	Dobin et al., 2013	N/A
outadapt 1.14	Martin, 2011	N/A
Max Quantvl.6.0.16	Cox et al., 2014	N/A
MSstats v4.0.0	Choi et al., 2014	N/A
imputeLCMD v2.0	Lazar, 2015	N/A
limma v3.48.0	Ritchie et al., 2015	N/A
deepTools 3.1.1	Ramírez et al., 2016	N/A